Accepted Manuscript

Journal of the Geological Society

Were springline carbonates in the Kurkur-Dungul area (Southern Egypt) deposited during glacial periods?

Sándor Kele, Emad S. Sallam, Enrico Capezzuoli, Mike Rogerson, Hamdalla Wanas, Chuan-Chou Shen, Mahjoor Ahmad Lone, Tsai-Luen Yu, Andrew Schauer & Katharine W. Huntington

DOI: https://doi.org/10.1144/jgs2020-147

To access the most recent version of this article, please click the DOI URL in the line above. When citing this article please include the above DOI.

Received 29 July 2020
Revised 8 December 2020
Accepted 14 December 2020

Supplementary material at https://doi.org/10.6084/m9.figshare.c.5246661

Were springline carbonates in the Kurkur-Dungul area (Southern Egypt) deposited during glacial periods?

Sándor Kele[1*#], Emad S. Sallam[2], Enrico Capezzuoli[3], Mike Rogerson[4], Hamdalla Wanas[5,6], Chuan-Chou Shen[7,8,9], Mahjoor Ahmad Lone[7,8], Tsai-Luen Yu[7,8], Andrew Schauer[10], Katharine W. Huntington[10]

[1]Institute for Geological and Geochemical Research, Research Centre for Astronomy and Earth Sciences, H-1112 Budapest, 45 Budaörsi út, Hungary, keles@geochem.hu
[2]Geology Department, Faculty of Science, Benha University, Farid Nada Street 15, Benha 13518, Egypt
[3]Department of Earth Sciences, Univ. of Florence, Via La Pira 4, Firenze, Italy
[4]Department of Geography and Environmental Science, Northumbria University, Newcastle, NE1 8ST, UK
[5]Department of Petroleum Geology and Sedimentology, King Abdulaziz Univ., Jeddah, Saudi Arabia
[6]Geology Department, Faculty of Sciences, Menoufiya University, Shebin El-Kom, Egypt
[7]High-Precision Mass Spectrometry and Environment Change Laboratory (HISPEC), Department of Geosciences, National Taiwan University, Taipei, 10617 Taiwan ROC
[8]Research Center for Future Earth, National Taiwan University, Taipei 10617, Taiwan, ROC
[9]Global Change Research Center, National Taiwan University, Taipei 10617, Taiwan, ROC
[10]Department of Earth and Space Sciences, University of Washington, Seattle, WA 98195, USA

Abstract

The tufa deposits in the Kurkur–Dungul area, southern Egypt, date from marine isotope stage (MIS) 11 to MIS 1. Springs across the region were active during glacial periods (with sea level below –50 m), reflecting changed atmospheric circulation over the Indian Ocean, as well as peak interglacial periods. During times of low sea level, reduced Indonesian throughflow promoted formation of an Indian Ocean Warm Pool, and anomalous rainfall on its western margin. We suggest Egypt lies at the intersection of westerly ("maghrebian") and easterly ("mashriqian") rainfall provinces, which show different timing with relation to orbital forcing and different source water regions. Tufa-growth periods are therefore not mechanistically linked to "humid periods" or "sapropel events" identified elsewhere. Stable isotope and $T_{\Delta 47}$ data are also inconsistent with these spring systems being part of a larger system spanning northern Africa, and lack a clear interaction between northern hemisphere heating and mid-latitude rainfall. We also follow previous authors in concluding that formation of springline deposit formation was likely delayed compared to rainfall, due to aquifer flow distances. This delay is unlikely sufficient to explain why rainfall is out of phase movements of the monsoon belts, but may complicate interpretation of these records.

Keywords: Desert tufa; Southern Egypt, Facies analysis; Stable and clumped isotopes; U−Th dating

Tufas are terrestrial carbonates that form under open air conditions at ambient temperature from calcium-bicarbonate water in streams, rivers and lakes, thus they indicate active spring lines or water table intersection with the ground surface and meteoric water recharge (Pedley 1990; Andrews 2006). Tufa and travertine (similar deposits forming in geothermally warmed springs) have been used to study palaeoclimatic, tectonic and palaeoenvironmental conditions on local, regional and global scales (Chafetz and Folk 1984; Ford and Pedley 1996; Hancock *et al.* 1999; Arenas *et al.* 2000; Andrews 2006; Capezzuoli *et al.* 2010; Özkul *et al.* 2013; Török *et al.* 2017; Della Porta *et al.* 2017a; Toker 2017). Egyptian tufa studies have focused on palaeohydrology, palaeoclimate and hominin dispersals (e.g. Crombie *et al.* 1997; Smith *et al.* 2004a, b; Drake *et al.* 2013). As shown by

the sporadic presence of tufa and speleothems indicates, the areas of the Saharan and Arabian deserts were not always as arid as they are today (5−20 mm/y rainfall; Burns and Matter 1995; Osmond and Dabous 2004; Patterson *et al.* 2005; Cremaschi *et al.* 2010; Dramis *et al.* 2014; Dramis and Fubelli 2015; El-Shenawy *et al.* 2018; Fleitmann *et al.* 2003; Drake *et al.* 2013; Nicoll and Sallam 2017). Dating and geochemical study of these tufa can elucidate these past humid periods, recording information about the type of recharge, moisture source origins and relationships with larger scale changes in the climate system. In Egypt, previous studies provided important information about tufa and travertine deposits (Butzer 1964; Ahmed 1996; Anwar 2004; Adelsberger and Smith 2010; Smith 2012; Sallam *et al.* 2018; Sallam and Ruban 2019), and some studies (Crombie *et al.* 1997; Sultan *et al.* 1997; Smith 2001; Wanas 2012; Hassan 2014; Jimenez 2014; Hassan 2015; Hamdan and Brook 2015; Abotalib *et al.* 2016; Nicoll and Sallam 2017; Gaber *et al.* 2018) utilised stable isotopes to reconstruct the temperature or $\delta^{18}O$ of the precipitating water. However, the timing of humid periods compared to forcing (which is expected to underlie change in rainfall in the region) is still debated, and research progress has been challenged by uncertainties due to assumptions regarding the $\delta^{18}O$ or T values of the precipitating water, and because of kinetic fractionation during tufa deposition. As a result, there are critically important open questions regarding the moisture source, the ambient temperature during deposition and the processes controlling the North African climate throughout the Pleistocene and Holocene.

In the Western Desert in Egypt, several oases (e.g. Kurkur, Dungul, Farafra, Khraga, and Dakhla) host travertine and/or tufa deposits (Crombie *et al.* 1997; Sultan *et al.* 1997; Kleindienst *et al.* 1999; Smith *et al.* 2007; Jimenez 2014; Wanas and Armenteros 2019). This study addresses the sedimentological and geochemical aspects of these tufa systems, including their lithofacies and depositional environments. We focused on the Kurkur, Dungul and Dineigil oases, as well as the Gebel Kalabsha and Gebel El−Digm mountains located in-between and used petrographic, stable-carbon and oxygen isotope, clumped isotope, and U−Th age data of tufa deposits to 1) date and reconstruct the palaeoclimatic conditions prevailed in southern Egypt during the Quaternary, 2) understand the palaeoenvironmental conditions of tufa formation, and 3) determine the temperature and origin of the tufa depositing water (the source of precipitation).

Geological setting

The Kurkur-Dungul area is located in southern Egypt along the eastern part of the south Western Desert between latitudes 24° and 23° 22′ N and longitudes 31° and 32° 46′ E and includes parts of the Nubian plain (**Fig. 1**). The study area comprises the Kurkur, Dungul and Dineigil Oases as well as Gebel Kalabsha and Gebel El−Digm. Kurkur Oasis is located about 62 km southwest of Aswan City in southern Egypt between lat. 23° 54' N and long. 32° 19' E. Dungul Oasis (region centered at lat. 23° 25' N and long. 31° 36' E) is considerably smaller than Kurkur Oasis. It lies about 60 km to the west of Kurkur Oasis, in a topographically low area in Wadi Dungul. Wadi Dungul collects rain water from the surrounding plateau surface where dendritic drainage networks are well developed. The water trapped in Dungul feeds springs located in the main deprerssion of the wadi. The study area in-between Kurkur and Dungul oases comprises two mountains (Gebel Kalabsha to the east and Gebel El−Digm to the west) forming a part of the scarp face of the Sinn El−Kaddab Plateau. Dineigil Oasis is a small basin lying about 7 km south of the Dungul Oasis on a step of the plateau surface near the scarp face.

The area is dissected by numerous deep-seated strike-slip and dip-slip faults, mainly in E-W and N-S directions (Issawi 1968). The E–W trending faults dissect the limestone plateau of Sinn El-Kaddab forming several horsts and grabens, and some major faults (e.g.,

Kalabsha fault) extend into the Nubia plain. The N-S trending faults primarily dissect the sandstone beds of the Nubia Formation, but can also affect the limestone plateau areas (Issawi 1968; Khamies and El-Tarras 2010).

The Kurkur–Dungul area exposes a thick sedimentary succession deposited on a corrugated surface of Precambrian rocks. This succession, ranging in age from the Late Cretaceous to the Quaternary (**Fig. 1, Fig. S1**) (Issawi 1968; Van Houten *et al.* 1984; Nicoll and Sallam 2017), is made up of thick fluvio-marine to near-shore marine deposits (Nubia Fm – Coniacian−Santonian; Issawi 1968; Van Houten *et al.* 1984; Khamies and El-Tarras 2010) that are conformably overlain by near-shore marine gypsiferous shale (Dakhla Shale – Maastrichtian; Said 1961; Issawi *et al.* 2009). Towards the top, the latter formation comformably passes to shallow marine fossiliferous limestone with sandstone intercalations (Kurkur Fm – Paleocene; Issawi 1968). An unconformity marks the passage to the uppermost marine limestone, chalky limestone and shale (Garra Fm – Paleocene-Early Eocene) and reefal limestone (Dungul Fm - Early Eocene) testifying to the termination of the southward transgression of the Neo-Tethys over Egypt (Issawi 1968).

The Quaternary deposits in the Kurkur–Dungul region were classified by Issawi (1968) as: 1) conglomerate sheets, 2) freshwater carbonates (tufa and travertine), 3) freshwater limestone mapped from Gebel El−Digm, 4) calcareous deposits covering some wadi channel banks in-between Gebel Kalabsha and Gebel El−Digm, 5) mudpans covering the pediplain between the Nile and the Sinn El−Kaddab scarp, and 6) sand dunes developed in arid intervals during the late Quaternary.

The Nubian Aquifer

The Nubian aquifer extends over a large area including northern Sudan, Eastern Libya, and Western Egypt (Sultan *et al.* 1997) and two sites have been proposed as recharge regions: the southwest mountainous areas and the desert itself under conditions more humid than today (Sanford 1935; Thorweihe 1982).Tufa deposits in the Kurkur-Dungul area were precipitated from springs from perched aquifers above this main Nubian Aquifer System during wet periods when water table was significantly higher (Nicoll and Sallam 2017). In this scenario, past pluvial episodes recharged the Nubian Aquifer in the southern areas, causing deep groundwaters move in a northwest direction. Consistent with this view, Jimenez (2014) compared tufa geochemistry ($^{87}Sr/^{86}Sr$, stable isotopes) with modern groundwater chemistry and suggested a consistent Nubian groundwater source over the last 500 ky in the Western Desert with some deeply-derived component. Retention time for water in the aquifer is at least several 100 ky (Gossel *et al.* 2010; Sherif *et al.* 2019) reflecting slow rates of flow (0.5−3.5 m/y), and residence time may be as high as 1.3 Ma (Sturchio *et al.* 2004; Patterson *et al.* 2005; Jimenez 2014). Throughout the last million years, the hydrologic conditions have changed several times in the recharge areas, mixing of water from different times and different sources (Gossel *et al.* 2010). Between 300 and 1000 ky, infiltrating precipitation also underwent evaporation and condensation processes, further complicating its isotopic and compositional characteristics (Gossel *et al.* 2010). Quantitative work by Gossel et al. (2004) and Voss and Soliman (2014) has shown that 1) 5500 yr is needed from the beginning of a wet period for an aquifer to recharge completely, 2) groundwater levels begin to decline in depressions 1000 years after termination of wet periods, 3) and up to 10 ky (or even more) is needed for natural groundwater discharge to cease (Abotalib *et al.* 2019).

Material and analytical methods

Sampling

Tufa and calcite deposits located at different elevations in five locations (**Table S1**) along the Kurkur–Dungul area were lithologically classified and sampled (**Table S2**; **Fig. S2, S3**). These locations are the Kurkur Oasis (**Fig. S4**), Gebel El-Digm (**Fig. S5)**, Dineigil Oasis (**Fig. S6**), Dungul Oasis and Gebel Kalabsha (**Fig. S7**). From each location, several samples were collected from each lithofacies and from different topographic elevations. Forty-five thin sections, representing a selection of all the identified lithofacies, were prepared and examined under Olympus BX51 light microscopy. This allows the avoiding of secondary cements and diagenesis and the choosing of the best samples for geochemical analyses.

Stable isotope analyses

Eighty-two stable (oxygen and carbon) isotope analyses from 74 carbonate rock samples (tufa or primary cement "calcite" materials) were determined using an automated carbonate preparation device (Gasbench II) and a Thermo Fisher Scientific Delta Plus XP continuous flow mass spectrometer at the Institute for Geological and Geochemical Research, Budapest, Hungary. Carbonate powders were extracted with a dental microdrill avoiding the mixing of carbonate components and were reacted with 100% phosphoric acid at 70 °C. Standardization was conducted using laboratory calcite standards calibrated against the NBS−19 standard. The carbon and oxygen isotopic compositions are expressed in the conventional delta notation against the international standard V−PDB (for $\delta^{13}C$ and $\delta^{18}O$). One-sigma reproducibility for both C and O isotope analyses is better than ± 0.1‰.

Clumped isotope analyses

Clumped, carbon, and oxygen isotopic composition of bulk carbonate powder of ten tufa carbonate and primary calcite cement samples were measured at the University of Washington's IsoLab (U.S.A.). The details of the automated vacuum line and sample purification methods used in IsoLab are described in Burgener *et al.* (2016). In this work 6−8 mg of powdered subsample was reacted in a common acid bath at 90ºC and cryogenically purified using an automated system. Purified CO_2 was analyzed using a multi−collector MAT253 IRMS (Thermo Scientific) configured to measure masses 44−49 inclusive. Reference gas piped into this instrument eliminated the need for reference gas refilling, and ensured sample and standard are balanced throughout a run. The correction for ^{17}O interference used a value of 0.528 to relate abundances of ^{17}O and ^{18}O (Brand *et al.* 2010), which has been shown to increase the accuracy of Δ_{47} and eliminate discrepancies among abiogenic Δ_{47}−temperature calibrations (Schauer *et al.* 2016). Pressure baseline correction (He *et al.* 2012) was made by measuring the reference gas signal 0.0084V down voltage of the peak center. Samples were converted to the carbon dioxide equilibrium scale (CDES) Δ_{47} reference frame (Dennis *et al.* 2011) using a suite of CO_2 samples equilibrated with deionized and isotopically enriched water at 4, 60 and 1000ºC. All Δ_{47} values reflect 90ºC acid digestions with the application of an acid fractionation factor to approximate a 25ºC reaction. Long−term Δ_{47} precision based on repeat measurements of an in−house calcite standard is ±0.018‰ (1 σ). Sample reproducibility is taken as the standard error calculated using the number of sample replicates and the standard deviation (SD) of sample replicates or the SD of carbonate standards, whichever is larger. Both of these values can be found in the EarthChem archived file (**Kele et al. 2020**).

U−Th dating

From each locality (**Fig. S2, Fig. 2**) the cleanest samples were selected for dating. Eleven tufa samples were dated with U–Th techniques at the High–Precision Mass Spectrometry and Environmental Change Laboratory (HISPEC), Department of Geosciences, National Taiwan University (Shen *et al.* 2003, 2012). For each sample, bulk and clean 1–2 g subsample was selected, gently crushed, ultrasonicated and then dried at 50 °C on a class−100 bench in a class 10,000 clean room (Shen *et al.* 2008). The cleanest fragments, 0.1–0.7 g, were picked for U–Th chemistry (Shen *et al.* 2003). A triple–spike, ^{229}Th–^{233}U–^{236}U, isotope dilution method (Shen *et al.* 2002) was used to determine U−Th isotopic and concentration data. Instrumental analyses were carried out on a multi–collector inductively coupled plasma mass spectrometer (MC–ICP–MS), Thermo Electron Neptune (Shen *et al.* 2012). Uncertainties in the U–Th isotopic data were calculated offline (Shen *et al.* 2002) and include corrections for blanks, multiplier dark noise, abundance sensitivity, and contents of the four nuclides in spike solution. Half−lives of U−Th nuclides used for age calculation, relative to 1950 AD, are given in Cheng et al. (2013).

Tufas from paludal and pool environments usually contain significant detrital contamination, and this, combined this with low initial U concentrations and short time for ingrowth of radiogenic ^{230}Th make high-resolution U-series dating of tufa extremely challenging (Garnett *et al.* 2004). The very low concentrations of authigenic ^{230}Th mean that even slight variations in the initial ^{230}Th/^{232}Th value of the detrital component can have a large impact on the calculated age (Garnett *et al.* 2004). In this study age corrections for initial detrital ^{230}Th content were calculated using an estimated atomic ^{230}Th/^{232}Th ratio of 4 (± 2) x 10^{-6}; those are the values for a material at secular equilibrium, with the crustal ^{232}Th/^{238}U value of 3.8 and an arbitrary uncertainty of 50%. Isotopic and age errors given are two standard deviations of the mean and two standard deviations, respectively, unless otherwise noted.

Results

Lithofacies description

Seven main lithofacies (FA1 to FA7) were recognized and their description and classification are summarized according to the terminology of Gandin and Capezzuoli (2014) and Della Porta *et al.* (2017a) (**Table S2, Text S-1 and Fig. S8**).

The lithofacies are mainly characterized by tabular Clotted peloidal mudstone/wackestone (FA1), hemidomic Laminated boundstones (FA3) and local Micritic dendrite boundstone (FA6). In the marginal portions, lenticular-to-tabular Coated plants boundstones (FA4) and Crystalline dendrite boundstone (FA2) become predominant. Intraclastic rudstones/packstones (FA5) are present at the wadi margins and locally intercalated in the more distal portions. Only at Gebel Kalabsha, blocky primary calcite cements are present along local fractures as crusts and druses (FA7).

Stable isotopes

δ^{13}C and δ^{18}O values range between −9‰ and −1.1‰ and between −13.3‰ and −8.5‰ (V−PDB), respectively (**Table S3, Fig. 3)**. The highest δ^{13}C values were measured from sites 1 and 2 of Kurkur Oasis and site 5 of Dungul Oasis, while the lowest values were from the calcite samples from Gebel Kalabsha ($\delta^{13}C_{average}$= −7.3‰) and a calcite part of a country rock from Gebel Kalabsha ($\delta^{13}C_{average}$= −5.3‰). The lowest $\delta^{13}C_{tufa}$ values are from the Coated plants boundstone tufa of the Dineigil Oasis ($\delta^{13}C_{average}$= −5.9‰) (**Fig. 3**). δ^{13}C and δ^{18}O values of four primary calcite cement samples from Gebel Kalabsha range between

−9.0‰ and −6.3‰ and between −11.8‰ and −11.3‰, respectively. The rock part and the vein and vug-filling calcite of a country rock sample (CR 1, **Fig. 3**) of Gebel Kalabsha were also analysed separately ($\delta^{13}C_{rock}$ = −5.2‰ and $\delta^{13}C_{calcite}$ = −5.3‰; $\delta^{18}O_{rock}$ = −11.9‰ and $\delta^{18}O_{calcite}$ = −12.3‰). Average $\delta^{13}C$ and $\delta^{18}O$ values of tufa samples from the Kurkur Oasis, Dungul Oasis and Gebel El−Digm are similar, as well as the average $\delta^{18}O$ value of tufa samples from Dineigil Oasis (**Fig. 3**). Calcite samples from Gebel Kalabsha have values around −11.5‰ and the lowest $\delta^{18}O$ value (−12.3‰) was measured from the calcite part of a country rock sample (**Table S3**, **Fig. 3**). Only the Coated plants boundstone tufa of the Dineigil Oasis and the crystal calcite samples of Gebel Kalabsha show deviation from the average tufa values (**Fig. 3**).

Most of the locations from which more than two samples were analyzed show strong positive correlation between the $\delta^{13}C$ and $\delta^{18}O$ values. At sites 4, 5 and 6 at Kurkur strong correlation ($r^2 > 0.85$) exists between the $\delta^{13}C$ and $\delta^{18}O$ values (**Fig. 3**) and in case of Kurkur, site 1 and site 3 the r^2 is +0.58 and +0.7, respectively. From Kurkur, site 7 only two samples were measured, while at site 2 no correlation was observed. At Dineigil Oasis the $\delta^{13}C$ and $\delta^{18}O$ values show slight correlation (r^2 = +0.33) similarly to Gebel El−Digm, while samples from site 2 of Dungul Oasis show very strong correlation (r^2 = +0.98) (**Fig. S9**).

$\delta^{13}C$ value of all carbonate samples (**Table S3**) are in the meteogene range of Pentecost (2005). The empirical equation of Panichi and Tongiorgi (1976) resulted $\delta^{13}C_{CO2}$ values between −17.9 and −12.3‰ (V−PDB), while the theoretical equation of Bottinga (1968) provided similar values (from −17.5 to −11.0‰) (**Table 1**).

Clumped isotopes

Δ_{47} values of ten selected samples from Gebel Kalabsha, Kurkur−, Dungul−, Dineigil Oases and Gebel El Digm range between 0.658 ± 0.017‰ and 0.715 ± 0.012‰ (**Table 1**), corresponding to a temperature range between 36 and 16 °C, using the calibration of Petersen *et al.* (2019). Temperature uncertainties are on the order of 3 °C (1 standard error, or ~6 °C, 95% confidence interval). Kurkur 5−2 and Kurkur 6−3 samples were collected from sites where possible kinetic effects could have been present based on the strong correlation between the $\delta^{13}C$ and $\delta^{18}O$ values (**Fig. 3**). However, these two samples do not show significantly different temperature values from the other samples. Although the studied sites are located relatively close to each other, there are significant differences in the calculated temperatures (**Fig. S10**). The highest temperatures are from the fracture filling crystalline calcite from Gebel Kalabsha (36 °C) and from the tufa of Gebel El-Digm (33−34 °C), while the lowest temperature (16 °C) is from a tufa from Dineigil Oasis.

U−Th age data

Nine samples provide reliable U−Th age data from 368 ± 14 ky to 11.7 ± 1.2 ky (**Table 2**). From the Kurkur Oasis four samples were dated between 326 ± 14 ky and 139 ± 11 ky, while the two samples from Gebel El−Digm show relatively old ages (368 ± 14 ky and 258 ± 20 ky). Tufa samples of the Dungul Oasis were dated as 184.4 ± 5.4 ky and 43.52 ± 0.23 ky, while the youngest age of 11.7 ± 1.2 ky is from the Dineigil Oasis. At Dungul Oasis, the Dungul 12−1 sample (43.52 ± 0.23 ky) located at the lowest elevation (243−250 m a.s.l.), while the Dungul 16−5 sample (184.4 ± 5.4 ky) located at the highest elevation (302 m a.s.l.) (**Fig. 2**). At Gebel El-Digm, the sample located at the lowest elevation (Gebel El-Digm 9−6, 310 m a.s.l., 258 ± 20 ky) is younger than the Gebel El-Digm 11−2 sample located at 350 m a.s.l. (368 ± 14 ky). At Kurkur Oasis, the Kurkur 2−2 sample located at the lowest elevation

(272 m a.s.l., 139 ± 11 ky) is the youngest, while the Kurkur 5−2 sample (350 m a.s.l., 251 ± 4.7 ky) is older. However, the Kurkur 7−1 sample located highest (375 m a.s.l.) is younger then the Kurkur 6−3 sample located at 330 m (a.s.l.) with age of 326 ± 14 ky.

Discussion and interpretation

Depositional environment interpretation

The lithofacies recognized (see **TEXT S-1**) suggest slow sedimentation at ambient temperatures in low-energy environments. These environments include stagnant ponds, pools and shallow lakes, palustrine and/or lacustrine shores, water cascades, and at the margin of low-energy continental carbonate depositional system in dammed areas. Tufa mounds are concentrated along fault planes and seem to be formed by the circulation and emergence of carbonate-rich paleosprings through fissures and cracks during periods of enhanced groundwater discharge (Nicoll and Sallam 2017). Outgassing of CO_2 from carbonate-rich waters was an important factor in the formation of tufas along the paths of water streams, and particularly at water cascades where tufa deposition continually raised the profile of the stream, creating a positive feedback system (Nicoll *et al.* 1999; Nicoll and Sallam 2017). The clotted peloidal tufas (Kurkur Oasis, sites 1, 2) indicate deposition in ponded water areas subjected to wave action and turbulent currents or flowing water in gently sloped-stepped channels (Della Porta 2015). Carbonate-cemented intraclasts and gravels at the wadi margins (Kurkur Oasis, sites 1, 2) could have been deposited during the beginning of a humid period when surface runoff flushed loose debris into the wadi (Crombie *et al.* 1997) reflecting aggradation in slow-flowing water environments (dammed areas, pools, shallow lakes). The increasingly humid conditions raised the water table and led to carbonate precipitation in the wadi channel and in shallow lakes and pools at the confluence of wadi branches. Carbonate molds and casts of mosses (Kurkur Oasis, sites 3, 4, 5, 6) indicate deposition in stagnant pools or slow-flowing palustrine areas (Pedley 2009, Arenas-Abad *et al.* 2010), within interchannel areas, lacustrine shores, and the parts of terraces that were subjected to periodic water splash (Nicoll and Sallam 2017). The presence of Crystalline dendrite boundstone in the proximal parts of some sites (Kurkur Oasis, sites 4, 6) indicates deposition in fast-flowing, smooth to stepped slopes, and rims of pools (Jones and Renaut 2010). Localised "shrubby" facies at these same sites implies higher mineralization rate than is typical for ambient-temperature tufa sites, and/or involvement of microbial mats metabolizing reduced Sulphur (Erthal et al. 2017). Consequently, it is possible there was some geothermal influence at Kurkur, although this is unlikely to be above 35°C as this would inhibit the mosses and other macrophytes which are abundantly preserved in these materials. Crystal calcite crusts, primary cements and druses at Gebel Kalabsha are derived from local deposition of waters along fractures, and likely occurred below surface.

Age of tufa deposits

There is a poor correlation of Egyptian tufa dating to expected periods of rainfall in the Mediterranean basin derived from the understanding of marine sapropels. Our youngest tufa (Dineigil 8–4 sample, 11.7 ± 1.2 ky, marine isotope stage (MIS) 1/MIS 2 interglacial, **Table 2**) is likely too old to be ascribed to several humid periods that have been inferred at the start of the Holocene. For instance, this sample is older than sapropel S1 (10.5 to 6.1 ky) and the high African Monsoon Index of that time (Rossignol-Strick and Paterne 1999; Vaks *et al.* 2010; Grant *et al.* 2017) arising from either high northern hemisphere summer insolation (Laskar *et al.* 2004). It is also older than widespread African humidity of the early

Holocene (Szabo *et al.* 1995; Churcher *et al.* 1999; Kindermann *et al.* 2006; Geyh and Thiedig 2008; Brookes 2010; Drake *et al.* 2011; Hamdan and Lucarini 2013; Hamdan and Brook 2015; Kleindienst *et al.* 2016). Similarly, it is older than the closest phase of growth in speleothems from Hoti cave (10.5 to 6.2 ky, Burns *et al.* 2001) and Mukalla cave (10 to 6 ky, Fleitmann *et al.* 2011) or early Holcene low $\delta^{18}O$ values of Soreq cave speleothems (Bar-Matthews *et al.* 2003) (**Fig. 4**). Late Pleistocene and Holocene carbonates (McCool 2019), pedogenic carbonate concretions (Dal Sasso *et al.* 2018) and fossil gastropod shells (Williams *et al.* 2010) dated to 15–5 ky BP by AMS radiocarbon and ascribed to the African Humid Period are reported from the central and northern Sudan. From the Fezzan Basin (SW Libya) optically stimulated luminescence (OSL) data of lacustrine sediments inferred the existence of at least one perennial lake (Palaeolake Shati) between 11 and 9 ky (Armitage *et al.* 2007; Drake *et al.* 2008). The global early Holocene "travertine" age data frequency peak at around 8.6 ky (Ricketts *et al.* 2019), with "travertine" in that study being synonymous with "tufa" in this study. Again Dineigil age is older, placing it outside of the global trend to greater humidity at the start of the Holocene.

Similarly, the Dungul 12–1 tufa sample (43.5 ± 0.2 ky, glacial, MIS 3c, **Table 2**) does not fit to the sapropel events and is in the middle of a dry period in Northwest and East Africa (Grant *et al.* 2017), although it does fit one of the main travertine age data frequency peaks (at 41 ky) and occurs within the timeframe of inferred increased monsoon intensity from 40 to 50 ky (Ricketts *et al.* 2019) (**Fig. 4**). This period of humidity is not reflected to the further north and east, as Soreq cave speleothems (Bar-Matthews *et al.* 2003) show high $\delta^{18}O$ values and no dated speleothems are known from the Negev desert (Vaks *et al.* 2010), Hoti cave (Oman, Burns *et al.* 2001), or Mukalla cave (Yemen, Fleitmann *et al.* 2011). Growth at Wanni Sannur cave (Egypt, El-Shenawy *et al.* 2018) at this time is also absent, and no North and East Saharan lacustrine deposits are known of this age (Szabo *et al.* 1995; Geyh and Thiedig 2008). In contrast, growth phases of speleothems from the Susah Cave (Libya) were documented from the period immediately before (37.5–33 ky) and after (52.5–50.5 ky) the deposition of the Dungul 12–1 sample (Hoffmann *et al.* 2016), reflecting greater humidity during MIS3 to the west, and spatial complexity in the wider region. The probability density function (PDF) analysis of OSL and U–Th dates from humid sites in North Africa combined with paleohydrological mapping suggest that during MIS 3 and the start of MIS 2 there were three brief periods of enhanced humidity and humidity peaks centered on 76 ky, between 92 and 129 ky (Drake and Breeze 2016). A humid (lacustrine) phase occurred in SW Libya during the Last Interglacial as well (Armitage *et al.* 2007; Thiedig *et al.* 2000) and OSL age data of Drake *et al.* (2011) show evidence for humidity and interconnected hydrological system during MIS 5 in the Sahara. However, no deposition of this age has been found in the Egyptian tufa systems we discuss here.

From the Kurkur Oasis, the youngest tufa age data (Kurkur 2–2, 139 ± 11 ky, glacial MIS 6a) dates to the Penultimate Glaxial Maximum, but is older than the youngest "Greening period" (centered at 128.5 ± 1.1 ky), as suggested by El-Shenawy *et al.* (2018) based on dating of Wadi Sannur Cave speleothems (**Fig. 4**). The age of the Kurkur 2–2 tufa is older than the S5, and significantly younger than the S6 sapropel (Grant *et al.* 2017). According to the ODP967 wet-dry index (Grant *et al.* 2017) this period was significantly more humid than today, and that is also reflected in the formation of North and East Sharan lacustrine deposits (Szabo *et al.* 1995; Geyh and Thiedig 2008), speleothems (e.g. Negev desert, Vaks *et al.* 2010) and tufa and travertine (Gaven 1982; Kleindienst *et al.* 1999, 2008; Smith 2001; Smith *et al.* 2004b; Smith *et al.* 2007). There is evidence for humidity during MIS 6 at 135, 154 and 180 ky in the north and east of the Sahara (Drake and Breeze 2016). In Wadi Shati (SW Libya) an extensive Pleistocene lake existed with highstands between 140 and 130 ky (MIS 5d and 5e) (Gaven 1982). Lacustrine terraces with abundant carbonate accumulated during

humid episodes at >420, 380–290, 260–205, and 140–125 ky, roughly coincident with the MIS 9, 7, and 5e interglacial periods (Cancellieri *et al.* 2016).

The age of the Dungul 16–5 sample is 184.4 ± 5.4 ky (glacial MIS 6e, **Table 2**), which was a period of runoff from North Africa according to Grant *et al.* (2017) although the age of this tufa falls between the S6 (175.63 ky) and S7 (197.53 ky) sapropels. From this period there are age data from the Hoti and Mukalla caves (Burns *et al.* 2001; Fleitmann *et al.* 2011) but there is no overlap with the "Greening period" (centered at 219.4 ± 7.3 ky) of El-Shenawy *et al.* (2018) (**Fig. 4**). There are, however, several papers documenting travertine and tufa deposition at this time (Sultan *et al.* 1997; Brookes 2010; Kleindienst *et al.* 2016; Abotalib *et al.* 2019). $\delta^{18}O$ of speleothems from the Peqiin cave (Bar-Matthews *et al.* 2003) are high during this time period, implying aridity to the north of Egypt.

The Kurkur 5–2 sample is 251.1 ± 4.7 ky old (glacial MIS 8a, **Table 2**), which was a rather dry period according to Grant *et al.* (2017), and is not synchronous with any of the Greening Periods of El-Shenawy *et al.* (2018) (**Fig. 4**). This age is also slightly older than the S9 sapropel (241.35 ky, Grant *et al.* 2017). Dated speleothems from the nearby countries are reported only from the Mukalla cave (Fleitmann *et al.* 2011), however, lacustrine carbonates were present in the Northern and Eastern Sahara (Szabo *et al.* 1995; Geyh and Thiedig 2008).

The Gebel El-Digm 9–6 sample (258 ± 20 ky, glacial MIS 8b, **Table 2**) does not correspond to any of the sapropels, and Greening periods and dated speleothems are known only from the Mukalla cave (Fleitmann *et al.* 2011) (**Fig. 4**). This time period was dry in North Africa, as shown in Grant *et al.* (2017). However, lacustrine deposits are reported from the Northern and Eastern Sahara (Szabo *et al.* 1995; Geyh and Thiedig 2008), and a tufa sample from Gebel el Agouz was also dated to a similar age by Sultan *et al.* (1997).

The Kurkur 7–1 sample (283 ± 17 ky, interglacial MIS 9a, **Table 2**) does fit to a humid period of Grant *et al.* (2017) (**Fig. 4**). This timing is incompatible with the age of the S9 and S10 sapropels, and does not fit with the Greening Periods of El-Shenawy *et al.* (2018) or with humid periods recorded in speleothems (Burns *et al.* 2001; Vaks *et al.* 2010; Fleitmann *et al.* 2011; El-Shenawy *et al.* 2018). However, East Saharan lacustrine deposits are mentioned by Szabo *et al.* (1995) and tufa samples from Gebel el Yabisa were dated from this age (Sultan *et al.* 1997).

The Kurkur 6–3 sample (326 ± 14 ky, interglacial peak, MIS 9e) is slightly younger than the age of S10 sapropel (334.83 ky, Grant *et al.* (2017) and the related humid period (**Fig. 4**) and partly overlaps with the Greening Periods and speleothem age data published from the Wadi Sannur cave (El-Shenawy *et al.* 2018), Negev Desert (Vaks *et al.* 2010), Hoti cave (Burns *et al.* 2001), Mukalla cave (Fleitmann *et al.* 2011) and North Saharan lacustrine deposits (Geyh and Thiedig 2008).

The Gebel El-Digm 11–2 sample (368 ± 14 ky, MIS 11a interglacial, **Table 2**) does not fit neither to any of the Greening Periods of El-Shenawy *et al.* (2018), nor to the speleothem age data and sapropel events reported above and it is right in a very dry period of Grant *et al.* (2017) (**Fig. 4**). However, Geyh and Thiedig (2008) report lacustrine deposits from the North Sahara and Armitage *et al.* (2007) reports a humid phase from Libyan Sahara (SW Libya), which was tentatively correlated with MIS 11.

Climatic significance of tufa growth timing

The poor correlation of the Egyptian tufa dating with expected periods of rainfall in the Mediterranean basin (derived from the understanding of marine sapropels described above) is surprising for a system that is expected to be driven homogenously by insolation-forced migration of the Intertropical Convergence Zone (ITCZ) (Bosmans *et al.* 2015). However, we find better coherence between tufa phases reported here and tufa, "travertine"

and lacustrine deposits further south in eastern Africa. The Kurkur area is among the driest areas on Earth and currently Kurkur Oasis has limited spring discharge (Butzer 1965; Nicoll and Sallam 2017), so we can be confident these deposits reflect regionally significant decrease in water deficit. Consequently, we are able to consider any period of significant tufa growth to be a direct result of significant increase in the recharge of the aquifer, which combined with the eastern African lake and tufa data requires a large region of increased rainfall. An important caveat provided by Abotalib *et al.* (2019) is uncertainty about whether aquifer recharge needs to be close to the site of tufa formation, or could reflect rain hundreds of km further south and referred through the exceptionally large Nubian sandstone aquifer. Because such transport of water would depend on recharge of these aquifers, this could delay formation of spring deposits by thousands of years, significantly altering interpretation of depositional ages. As emphasized by Abotalib *et al.* (2019), modelling of the Nubian Sandstone aquifer indicates that it may take ~5.5 ky from the beginning of a recharge period for the aquifer, and a 1 ky delay between the onset of arid conditions in the recharge area and significant groundwater level fall (Voss and Soliman 2014). These aquifer recharge dynamics would be expected to delay spring flow inception, and maximum tufa formation, potentially on the order of several thousand years. If the delay between the onset of arid conditions in the recharge area and the timing of maximum tufa formation is consistent through time, dating of tufa sites should therefore exhibit a probability peak with the same characteristic timing delay compared to atmospheric forcing.

We investigate this effect by exploring the timing of the deposits described herein relative to the orbital forcing which is expected to underlie changes in rainfall in the region. The primary driver of rainfall changes in the Sahara region is considered to be northern hemisphere insolation, specifically with excess warming of the northern hemisphere leading to more rainfall in currently arid and hyperarid regions (Grant *et al.* 2016). If growth of tufa deposits reflects rainfall distal from the site, transferred to a more northerly location and a later time by aquifer transport, tufa timing should be expected to follow peaks in northern hemisphere insolation (Berger *et al.* 2003).

The delay periods indicated in the upper part of **Table 3** are very variable, and some are so large as to almost place tufa formation onto the subsequent northern hemisphere insolation maximum. For example, Dineigil 8–4 actually leads northern hemisphere insolation, with a delay of –1.4 ± 1.2 ky. Other tufa formation phases have long (e.g. Dungul 12–1) or short delay periods (e.g. Gebel El-Digm 11–2 with a delay of 3.5 ± 14 ky), although dating uncertainty means these delays could still be >10 ky. On average, delay for the new data presented here is ~8.6 ky compared to the assumed forcing. Extending the same analysis to the literature review data compiled by Abotalib *et al.* (2019) is complicated by the use of different dating technologies and incorporation of different types of deposit in their analysis. For instance, playa deposits may arise from local pooling above a perched water table and reflect a smaller rainfall period which may not significantly recharge the aquifer. Restricting the analysis to tufa sites dated by the U–Th method, permits a realistic evaluation of apparent delays, and we find the pattern shown in the lower half of **Table 3**. Again, we find that these delays are very large and very variable (average 6.8 ky, range –0.3 ± 1.3 ky to 19.5 ± 2.8 ky). Even with 2σ error taken into account, three sites show delays >9 ky, which are difficult to explain even with a long aquifer recharge delay, and a further three sites show delays less than 5 ky even with 2σ error taken into account, which is more rapid than would be expected. Although it is possible that variable control on timing is arising from a complex interaction between orbital forcing and aquifer recharge dynamics, the long average delay, highly variable delay and the lead over forcing on the site we report with the best constrained date (Dinigeil 8–4) are all challenging for this conceptual model to explain.

One solution for this is that the forcing is more complex, and does not arise essentially

from precession-forced motion of the ITCZ. Similar to the results and interpretation of Abotalib *et al.* (2019), our new age data show tend to fall within glacial periods. This may be significant, as recent climate modelling (Di Nezio *et al*. 2016)] suggests that the emergence of the Sunda and Sahul shelves due to sea-level fall resulted in significant oceanographic and atmospheric reorganisation in the Indian Ocean region, which affected rainfall in eastern Africa. This reorganisation would result in periods of increased rainfall in eastern Africa during glacial periods when the Indonesian Throughflow was significantly reduced. Based on the depth of the majority of the Sahul and Sunda shelf areas, and also the depth of the Karimata Strait (Di Nezio *et al.* 2016), we estimate that significant reduction of the Indonesian Throughflow would occur due to sea levels fall of at 50 m or more below modern levels.

Seven of the nine sites we present have timings that place them within periods with sea level of at least –50 m, using the eustatic sea level curve presented by Grant *et al.* (2014) (**Fig. 4**). The remaining two have mean dates outside these periods, but uncertainties that extend into low sea level periods renders them ambiguous. Within the period analysed by Grant *et al*. (2014), periods with sea level at least as low as –50 m occur about 53% of the time. Laying the ambiguous sites aside, the probability that 7 sites would occur during low sea level periods and none would occur during high sea level due to random sampling is thus ~1%. Extending the same analysis to the data compiled by Abotalib *et al*. (2019), we find 10 sites (50%) which occur during low sea level and a further 3 (15%) ambiguous sites with uncertainty ranges extending into low seal level periods. All 7 of the remaining sites are of MIS5e age, and exhibit consistently low apparent delays to precession (an average of 1.0 ky and a maximum of 3.7 ± 3.6).

We find it challenging to conclude that a single forcing can underlie this pattern, and suggest that the simplest explanation is that there are at least two causes for flow at these spring sites: wet phases during very warm interglacials (MIS5e) and during glacial periods arise from different forcing factors. The very short and very consistent delay for the MIS5e sites suggests that these periods are not being significantly delayed by aquifer recharge processes, implying rather short distance between the site of rain and the tufa site itself. It is not possible to make a similar evaluation for the glacial mode, but if this period is being forced by a sea-level lowstand Indian Ocean Warm Pool, the rainfall arising from this would be expected to be located to the south of Egypt. Consequently, it is likely that periods of glacial tufa growth are delayed relative to the rainfall.

Indication of overall drying through the period of study

Gaber *et al.* (2018) measured $\delta^{13}C$ and $\delta^{18}O$ values of tufa samples from different elevations at Kurkur, ranging from Pleistocene (older upper level, ~345 m a.s.l.) to Recent (younger lower level, ~270 m a.s.l) and concluded that the old tufa had been developed during warm pluvial, while the young ones in drier periods. Jimenez (2014) obtained 76 ky to 246 ky for the lower levels and 514 ky for the higher levels of the travertines at Kurkur, and suggested deposition between 600 ky and 1 My as well. Based on Crombie *et al.* (1997) the youngest spring and lacustrine travertines (70−160 ky) were found in Wadi Kurkur, while 191−220 ky old deposits are exposed as linear mounds over fracture zones in ancient wadis and the oldest travertines (> 260 ky) are extensive units on the plateau surface, deposited in paludal and lacustrine environments. Our age data show good correlation (r^2 = 0.83) with elevation supporting the observations of Jimenez (2014) and Gaber *et al.* (2018) (**Table 2, Fig. S11**). In almost all cases, the oldest tufa is located at the highest position, while the younger samples are at lower positions, suggesting a progressive lowering in the water table with time (**Fig. 2**). This supports the original suggestion of Szabo *et al.* (1989) that the water

table levels declined in this region over the Pleistocene. Reduction of the intensity of humid episodes throughout the Pleistocene was suggested by Szabo *et al.* (1995), Smith *et al.* (2004b) and Brookes (2010), who confirmed a decreasing trend of the lacustrine sedimentation in NE Africa over time during the late Quaternary. In addition, Geyh and Thiedig (2008) report a trend of shrinking lake size across the Quaternary, that was even more pronounced in the Late Pleistocene and Early Holocene (Cancellieri *et al.* 2016).

Significance of Stable Isotope values in Egyptian tufa and calcite

Carbon and oxygen isotopic composition of tufas and travertines are useful for understanding the palaeoenvironmental and palaeoclimatological conditions that prevailed during their deposition (e. g., Andrews *et al.* 2000; Andrews 2006; Gandin and Capezzuoli 2008; Pedley 2009; Cremaschi *et al.* 2010; Capezzuoli *et al.* 2014; Teboul *et al.* 2016; Della Porta *et al.* 2017a, b; Pla-Pueyo *et al.* 2017), although the data can be affected by diagenesis. Covariations between the $\delta^{13}C$ and $\delta^{18}O$ of tufa (**Fig. 3**) would also likely arise from aridity gradients during deposition (higher balance of evaporation over precipitation would simultaneously enrich $\delta^{18}O_{water}$ and $\delta^{13}C$ derived from organic matter; Talma and Netterberg 1983). Heavy carbon isotope values can imply long residence of carbon isotope species in water and equilibration with atmospheric CO_2 (Andrews *et al.* 1993) and evaporation can induce ^{18}O and ^{13}C enrichment, thus covarying $\delta^{13}C$ and $\delta^{18}O$ values in lake systems (e.g. Talbot 1990; Horton *et al.* 2016). In case of Kurkur tufas, Nicoll and Sallam (2017) showed petrographic evidence for the lack of diagenetic features typical of a burial regime, and we find no indication of significant alteration in our thin section analysis beyond cementation. Such early diagenesis generally occurs in the same water the non-cement phases were deposited from, and this very early diagenetic impact on isotope geochemical proxies may be insignificant (Andrews and Brasier 2005; Andrews 2006; De Boever *et al.* 2017). It therefore seems likely that the isotope values established for these materials are a good indication of the water and carbon available at these sites at the time of deposition. More likely, the correlation between $\delta^{13}C$ and $\delta^{18}O$ in most of our sampled locations, together with our petrographic data, reflects evaporation, rapid degassing and related kinetic effects during deposition under an arid climate (Kele *et al.* 2008, 2011), which would have been exaggerated by the shallow pool environments which dominated these systems (see facies analysis in **TEXT S-1**). This reflects similar findings by Hassan (2015), who observed significant (r=+0.85) correlation between the $\delta^{13}C$ and $\delta^{18}O$ values of soil carbonates from the New Cairo Petrified Forest and interpreted it as a result of aridity and Gaber *et al.* (2018), who found very weak correlation between the $\delta^{13}C$ and $\delta^{18}O$ values of their tufa samples from Kurkur, and Wanas and Armenteros (2019), who observed moderate covariance in case of fluvial tufa at Farafra Oasis (Egypt). To conclude, although the positive covariance between the $\delta^{13}C$ and $\delta^{18}O$ values caused by local disequilibrium conditions are common in tufa samples, their isotopic composition do contain palaeoenvironmental and paleoclimatic information (e.g. Pazdur *et al.* 1988; Andrews *et al.* 2000; Kano *et al.* 2007; Pedley 2009; Cremaschi *et al.* 2010).

The calculated isotopically depleted $\delta^{13}C_{CO2}$ values (**Table 1**) suggest that the studied carbonates are mostly tufa samples deposited from meteoric waters associated with soil and atmospheric CO_2 characterized by low $\delta^{13}C$, with minimal crustal carbon addition (**Fig. 3**). This is also consistent with their sedimentary facies, which are dominated by features of ambient temperature systems with strong biomediation of precipitation, and even where some indication of warming is noted (as at Kurkur) the temperatures do not seem to have been raised above 30–35 °C. As we find no consistent relationship between facies and isotopic

characteristics, it seems precipitation kinetics and fractionation are rather coherent across these systems, and that disequilibrium effects are limited. Exceptions are 1) crystalline dendrite deposits (FA2 facies) showing the lowest $\delta^{18}O$ values (samples are mostly from the likely slightly geothermal Kurkur Oasis, sites 4, 5 and 6), which could be explained by deposition from low $\delta^{18}O_{water}$ (**Table 1**); 2) cement samples (Gebel Kalabsha) show the lowest $\delta^{13}C$ values (**Table S3, Fig. 3**) as they were probably less affected by evaporation than the pool samples, while their low $\delta^{18}O$ values could be the result of high (36 °C) temperature of deposition (**Table 1**).

Palaeoclimate Implications

Our $\delta^{13}C_{tufa}$ values (~ –6 to –1‰) are generally higher than the $\delta^{13}C$ values of other North African and Middle Eastern speleothems (Susah cave, Libya, Rogerson *et al.* 2019, –11 to –7‰; Soreq cave, Israel, Affek *et al.* 2008; –11 to –5‰, respectively) and partly overlap with the $\delta^{13}C$ values of the early Holocene tufa of Tadrart Acacus Mt. (SW Fezzan, Libya, –4.8 to 2.6‰, Cremaschi *et al.* 2010). However, the Egyptian values lie within the range of speleothems from the Negev Desert, Israel (Vaks *et al.* 2006, 2010, –9 to +1‰). The trend in the speleothems in the eastern Mediterranean climate region reflect trends in aridity, with $\delta^{13}C$ values between –12‰ and –8‰, reflecting C3 type Mediterranean vegetation, while the more ^{13}C-enriched range of the Negev reflects the C3–C4 mixed vegetation of the steppe and semi-desert (Vaks *et al.* 2006). We conclude that despite the evidence for increased spring flow, the environment in which these tufas were depositing remained an arid semi-desert, and that the rainfall providing the water may not be significantly altering the local landscape.

The youngest dated sample (Dineigil 8–4; **Fig. 4**) has the lowest $\delta^{13}C$ value (–5.9‰**)**, which is consistent with this being a humid period, reflecting a significant contribution of CO_2 from the soil zone derived from mixed C3/C4-type vegetation. This site also has relatively depleted $\delta^{18}O_{cc}$. It is likely that this deposit formed within a landscape more dissimilar, and less arid, than most of the sites investigated in this study. That finding is surprising, as this deposit formed during late MIS2, when the ITCZ is expected to be located far to the south of the Sahara. Our isotope data thus reinforces the conclusion from U-Th datings that this part of Egypt experienced important humid periods with different phasing to orbital forcing than is found in other systems. Clearly, the glacial eastern Sahara at least for short periods exhibited better water resources than are found in the current interglacial.

The $\delta^{18}O$ values of our dated Egyptian tufa samples (–12.7 to –8.9‰, **Table 1**) overlap with the most depeleted speleothem values reported by Vaks *et al.* (2006, –11.0‰ < $\delta^{18}O$ < –3.0‰) and by Vaks *et al.* (2010, –10.5‰ on average) from different caves of Negev Desert (Israel) and with the values published by Cremaschi *et al.* (2010) from the Holocene tufa of Tadrart Acacus (Libya, –11.3‰ < $\delta^{18}O$ < –2.1‰) (**Fig. 5)**. Soreq cave (Israel) speleothems have $\delta^{18}O$ values between –11.1 < $\delta^{18}O$ < – 5.2‰) (Affek *et al.* 2008), and similar ranges are reported from both the Mukalla cave (Yemen, –12.3‰ < $\delta^{18}O$ < –2.8; Fleitmann *et al.* 2011) and Hoti cave (–12‰ < $\delta^{18}O$ < –4‰; Burns *et al.* 2001). In both of those caves, the most depeleted values are reported during MIS5e. A stalagmite from the Wadi Sannur cave (El-Shenawy *et al.* 2018) has an $\delta^{18}O_{ave}$ value of –11.6 ± 0.8‰, which lies within the same range. Our $\delta^{18}O_{mean}$ tufa values are also very close to the $\delta^{18}O_{mean}$ data of lacustrine tufas from the Dungul region (−9.4‰, Hassan 2014) and to tufas of Kharga Oasis (−9.7‰, Smith *et al.* 2004a) (**Fig. S10**).

These datasets lie in strong contrast to Susah cave speleothems from Libya (Rogerson *et al.* 2019), where $\delta^{18}O_{cc}$ values are considerably higher (–5.3‰ < $\delta^{18}O$ < –3.8‰).

Pleistocene carbonates deposited in Libya, central Sahara have higher $\delta^{18}O$ values compared to our $\delta^{18}O_{tufa}$ values, although these will be modified by evaporation in a closed basin lake (Gaven *et al.* 1981). Nevertheless, the significant differences in speleothem data strongly implies two different hydrological provinces are active, one of which is located in central and western northern Africa ("maghrebian") and is isotopically enriched, and the other located in Egypt ("mashriqian"), which is isotopically depleted. The two isotopic provinces co-occur in the Arabia / Levant region, providing exceptionally large variances in records from these regions. It would seem likely that the relatively enriched isotopes recorded at Farafra oasis and the New Cairo Petrified Forest (**Fig. S10**) imply that the maghrebian isotopic province extends into northernmost Egypt. Indeed, it is possible that the rainfall driving tufa formation with mashriqian isotopic characteristics is in fact falling considerably further south, and the occurrence of this water in Egypt reflects aquifer transport.

The observation of an isotopic mixing zone in Egyptian palaeoclimate data is not itself new, having first been proposed by Smith *et al.* (2004a). In that original hypothesis, both westerly and Indian Ocean monsoonal precipitation contributed to the recharge of aquifers. The compilation of data in this study gives strong support to this concept, and reveals that rainfall in the region exhibits a much more complex spatio-temporal structure than has previously been appreciated. Although we support the suggestion of Smith *et al.* (2004a) that the maghrebian precipitation is likely "westerly", reflecting some Atlantic and considerable Mediterranean source moisture (Rogerson *et al.* 2019), the occurrence of mashriqian precipitation during MIS5e and during glacial periods makes a specific identification of this as "monsoon" rain difficult to sustain. It may reflect a mixture of monsoon and Indian Ocean Warm Pool-forced precipitation, which occur with different phasing compared to insolation.

Palaeotemperature

The average of our ten $T_{\Delta47}$ values (**Table 1**) is 29 °C, which is higher than the mean annual ground temperature (26.6 °C) of Egypt, but similar to groundwater temperatures in the Western Desert (26 to ~40 °C) (Swanberg *et al.* 1983). Lower temperatures (17.5 to 26.2 °C) are found by Abouelmagd *et al.* (2014), while 10 to 30 °C are inferred by Nicoll and Sallam (2017) for the tufas of the Kurkur region and by Hamdan and Brook (2015) for the Late Pleistocene Eastern Desert tufas (14 – 20.8 °C) and for the Holocene tufas at the same site (21 – 24 °C). Today, there are no thermal waters in the Western Desert, and waters with elevated temperatures are either artesian or pumped well waters arising from great depth (Crombie *et al.* 1997). The deep source at Kharga and Kurkur oases was supported by the Sr isotopic data of Abotalib *et al.* (2019), by the $^{234}U/^{238}U$ activity ratio and U concentrations of groundwater samples (Dabous and Osmond 2001) and by noble gas and geochemical analyses of springs and groundwater (Mohammed 2015). Swanberg *et al.* (1983) reported low (< 20 °C/km) regional temperature gradient in the Kharga, Dakhla, Farafra and Bahariya oases, and wells tapping deep artesian aquifers produce large volumes of water in the 35−43 °C range. High temperature values (29 − 53 °C) were measured by Sultan *et al.* (1997) on fossil groundwaters from wells that sample various horizons in the Nubian aquifer at Kharga, Dakhla, Farafra and Bahariya Oases.

Five out of our nine dated tufa samples deposited during glacial periods, while four samples formed during interglacials. Considering the interglacial samples, the Dineigil 8−4 sample formed during the MIS 1/MIS2 interglacial with a $T_{\Delta47}$ value of 16 ± 4 °C only, while the Kurkur 7−1 sample (MIS 9a), the Kurkur 6−3 sample (MIS 9e) and the Gebel El-Digm 11−2 samples (MIS 11a) formed at 30 ± 1, 30 ± 4 and 33 ± 2 °C, respectively. Samples from

glacials also scatter in their $T_{\Delta 47}$ data: Dungul 12−1 sample (MIS 3c) formed from a water of 22 ± <1 °C, but the other samples formed at higher temperatures (Kurkur 2−2, MIS 6a, 32 ± 7 °C; Dungul 16−5, MIS 6e, 27 ± 2 °C; Kurkur 5−2, MIS 8a, 34 ± 5 °C; Gebel El-Digm 9−6, MIS 8b, 34 ± 1 °C). The $T_{\Delta 47}$ values of our tufa samples thus do not follow the pattern of glacial-interglacial periods. This is consistent with mild geothermal heating affecting some or all of these sites inconsistently over time. It is worth noting that the facies showing most clear evidence of mild geothermal influence occurs at Kurkur, which also shows the most consistently high (30−34 °C) temperatures in clumped isotope measurements. In case of the Dungul Oasis the older sample, located at higher elevation is precipitated from a warmer (27 °C) water, than the one located at lower elevation (22 °C) (**Fig. 2**). At the other sites (e.g. at Kurkur) there is no relationship between the temperature of deposition and elevation. Thus, although there is a connection between the altitude of the samples and their age, this is actually not followed by the calculated temperatures.

Calculated $\delta^{18}O_{water}$ values

To properly resolve whether there are two precipitation isotopic provinces interacting in this region, we calculated $\delta^{18}O_{water}$ from $\delta^{18}O_{cc}$ data using the temperature constraints from clumped isotope thermometry (**Table 1**). These data indicate that the aquifer waters forming tufa deposits had $\delta^{18}O_{water}$ values between −9.7 and −6‰ using the Kim and O'Neil (1997) equation [or between −11.9 and −8.3‰ for the Kele *et al.* (2015) equation]. There is considerable uncertainty in these determinations however, as the average temperature uncertainty is 3 °C. When propagated into $\delta^{18}O_{water}$ alongside uncertainty in $\delta^{18}O_{cc}$ and calibration (we used a monte carlo approach, combining uncertainties in the measurement assuming they are all normally distributed), we find that the 1σ uncertainty is ~2‰ regardless of calibration equation.

Today, based on their stable isotope composition the waters in Egypt can be distinguished. Modern waters in an alluvial aquifer in northern Egypt are isotopically heavy ($\delta^{18}O$: +2.3 to +3.9‰, Bakri *et al.* 1992), while modern meteoric waters in Sudan have an average value of −2.1‰ (Joseph *et al.* 1992). Relatively young (<20 ky), shallow groundwaters have $\delta^{18}O$ values between −9.0 and −6.0‰ (Sonntag *et al.* 1978a, b; Haynes and Haas 1980; Muller and Haynes 1983). Old (>20 ky) Western Desert groundwaters have an average composition between −11.5 and −10.5‰ (Sonntag *et al.* 1978a, b; Thorweihe 1990; Sultan *et al.* 1997). Abotalib *et al.* (2016) analysed groundwater samples from the Bahariya Oasis, tapping the Nubian Aquifer ($\delta^{18}O$ from −11‰ to −10.3‰), and from Wadi El−Natrun and Wadi El−Farigh areas, tapping the Miocene and Pliocene aquifers ($\delta^{18}O$ from −2.4‰ to −1.3‰). Consequently, despite the wide uncertainty in our measurement this demonstrates that the springs we have analysed record waters consistent with "old western destert groundwaters", not younger groundwater, or older fossil groundwater tapping reservoirs emplaced in the pre-Pleistocene. This assists with placing our findings into regional context, as it demonstrates we are revealing conditions during the major humid periods that recharged the western desert aquifers, and that these conditions are not analogous to the modern climatology.

We come to the same conclusion when comparing reconstructed springwater $\delta^{18}O$ to modern rainwater isotope properties. The $\delta^{18}O$ of the rain water 15 km north from the New Cairo Petrified Forest (**Fig. S10**) was −8.2 to +5‰ from 1986−1991 to 2000−2003 (IAEA data, Hassan 2015). The weighted average value of $\delta^{18}O$ for present-day rain is −4.6‰ (OIPC data, Bowen 2008). This is also beyond the range of the values for palaeowater we provide, even given the range of uncertainty we have. This modern water is also more depleted in ^{18}O

than the water recorded in fluid inclusions of MIS 3 age from Susah Cave (Rogerson *et al.* 2019), although the wide range of possible values consistent with the data we present for Egyptian tufa does overlap with that range.

However, bearing the broad uncertainty range in $\delta^{18}O_{water}$ we report in our analysis and in this discussion, it is not possible to analyse differences between sites or times in detail.

Conclusions

This paper presents the first detailed geochemical study of Pleistocene tufa at Kurkur, Dineigil, Dungul oases, Gebel El−Digm and Gebel Kalabsha (southern Egypt), providing new U−Th ages and direct temperature and $\delta^{18}O_{water}$ estimations using the clumped isotope method. Based on stable isotopes and petrography the studied carbonates deposited from meteogene waters associated with soil and atmospheric CO_2 characterized by low $\delta^{13}C$ values. The observed facies associations (clotted peloidal mudstone/wackestone, crystalline dendrite boundstone, laminated boundstones, coated plants boundstones, intraclastic rudstones/packstones and micritic dendrite boundstones) suggest deposition in stagnant ponds, pools and shallow lakes, palustrine and/or lacustrine shores, and at the margin of low-energy depositional system in dammed areas. Stable isotopic compositions of the tufa samples are not significantly influenced by the facies. Correlation between the $\delta^{13}C$ and $\delta^{18}O$ values of tufa can be explained by kinetic effects caused by strong evaporation, in cases where the deposition occurred in shallow lakes, ponds. Facies analysis and clumped isotope geochemistry both suggest some slight geothermal heating at some sites / times, but not to the point vascular plants were excluded (30–36 ^{o}C).

The U−Th ages of the tufa are between 368 ± 14 ky and 11.7 ± 1.2 ky (between MIS 11 and MIS 1) indicating deposition during periods with low sea level (below –50 m). There is no consistent lag between tufa deposition and sapropel events, humid periods and speleothem deposition around the studied area, or to the expected orbital forcing (high northern hemisphere insolation). Rather, we suggest it likely that the region experienced spring flow during glacial periods. A potential explanation for this is that during low sea level, reduced Indonesian throughflow created an Indian Ocean Warm Pool, resulting in anomalous rainfall on its western margin. Tufas get younger towards lower elevations, indicating a progressive lowering of the water table level with time and therefore a long-term (million-year) trends towards greater aridity. Comparison with published datasets provides a regional picture which is compatible with this model of secular drying punctuated by glacial-age periods of aquifer recharge, with the exception of MIS 5e which appears to be the only high sea level period with substantial tufa development in Egypt.

The relatively high $\delta^{13}C_{tufa}$ values (–6.2‰ and –1.4‰) compared to the $\delta^{13}C$ of European tufa can be explained by contribution of mixed C3/C4 vegetation. Consequently, despite demonstrating a substantially increased amount of flow from the aquifer compared to today, the tufa deposits seem to have formed in semi-desert conditions comparable to the modern state. This is consistent with the argument by previous authors (Abotalib *et al.* 2019) that at least some of these deposits reflect rainfall further south, with water transported through the aquifer displacing the springs both from sites and times of enhanced rainfall.

The $\delta^{18}O_{tufa}$ values ($-12.7‰ < \delta^{18}O < -8.9‰$) are comparable to the values of tufa deposits from elsewhere in southern Egypt, but are incompatible with values for speleothems in Libya and tufa and associated deposits from northern Egypt. Combining data from our study and the literature, we support an argument from previous authors (Smith *et al.* 2004a) that Egypt lies at the intersection between two palaeoprecipitation provinces. These provinces display different $\delta^{18}O$ characteristics, with relatively enriched rainfall to the west reflecting Atlantic / Mediterranean sources (“maghrebian”) and relatively depleted rainfall to the east

reflecting an Indian Ocean source ("mashriqian"). The very large range of isotopes in speleothems recorded from Israel and Arabia may indicate rainfall from both sources within an intersecting zone.

Interpreting calculated $\delta^{18}O_{water}$ values is complicated by the propagated uncertainty arising from joint measurement of $\delta^{18}O$ and temperature via clumped isotopes. However, this approach demonstrates that the water depositing the tufa we report is inconsistent with modern rainfall in Egypt but is consistent with the water of Pleistocene age in western desert aquifers. This supports that rainfall in the past was not an analog of today in terms of moisture source.

Overall, we find that the record of climate in Egypts tufa is inconsistent with a simple model of palaeoclimate for this region. We find precipitation under both glacial and exceptionally warm interglacial times, but not during interglacials which exhibit lower global temperature rise. We also suggest that the region is responding to forcing related to the hydrology of the Indian Ocean, as well as from orbital forcing of movement in the ITCZ. Finally, we find that locations of spring formation are not necessarily locations of enhanced rainfall. Evidently, more field research into this region is needed to provide data further constraining this complex emerging picture.

Acknowledgements

S.K. received support by the KH 125584 project of the NKFIH (National Research, Development and Innovation Office, Hungary). Clumped isotope analyses at the Isolab (University of Washington, Seattle, USA) were supported partly by the TraRAS (Travertine Reservoir Analogue Studies) project, and K.H. acknowledges funding from the U.S. National Science Foundation grant EAR-1156134. The research was supported by the European Union and the State of Hungary, co-financed by the European Regional Development Fund in the project of GINOP-2.3.2-15-2016-00009 'ICER'. U-Th dating was supported by grants from the Science Vanguard Research Program of the Ministry of Science and Technology (MOST), Taiwan, ROC (108-2119-M-002-012), the Higher Education Sprout Project of the Ministry of Education, Taiwan, ROC (108L901001), the National Taiwan University (109L8926). Constructive comments made by Julian Andrews and an anonymus reviewer greatly improved the paper.

References

Abotalib, Z.A., Sultan, M., Elkadiri, R. 2016. Groundwater processes in Saharan Africa: Implication for landscape evolution in arid environments. *Earth-Sci. Rev.*, **156**, 108–136

Abotalib, Z.A., Sultan, M., Jimenez, G., Crossey, L., Karlstrom, K., Forman, S., Krishnamurthy, R.V., Elkadiri, R., Polyak, V. 2019. Complexity of Saharan paleoclimate reconstruction and implications for modern human migration. *Earth Planet. Sci. Lett.*, **508**, 74–84

Abouelmagd, A., Sultan, M., Sturchio, N.C., Soliman, F., Rashed, M., Ahmed, M., Kehew, A.E., Milewski, A., Chouinard, K. 2014. Paleoclimate record in the Nubian sandstone aquifer, Sinai Peninsula, Egypt. *Quat. Res.*, **81**, 158–167

Adelsberger, K.A., Smith, J.R. 2010. Paleolandscape and paleoenvironmental interpretation of spring-deposited sediments in Dakhleh Oasis, Western Desert of Egypt. *CATENA*, ***83***, 7–22

Affek, H.P., Bar-Matthews, M., Ayalon, A., Matthews, A., Eiler, J.M. 2008. Glacial/interglacial temperature variations in Soreq cave speleothems as recorded by

'clumped isotope' thermometry. *Geochem. Cosmochim. Acta,* **72**, 5351–5360

Affek, H.P., Matthews, A., Ayalon, A., Bar-Matthews, M., Burstyn, Y., Zaarur, S., Zilberman, T. 2014. Accounting for kinetic isotope effects in Soreq Cave (Israel) speleothems. *Geochem. Cosmochim. Acta,* **143**, 303–318

Ahmed, S.M. 1996. Geomorphic evolution and sedimentation of the tufa and travertine deposits in Kurkur Area, Southwestern Desert, Egypt. *Egyptian J. of Geol.*, **40**, 119–140

Andrews, J.E. 2006. Palaeoclimatic records from stable isotopes in riverine tufas: synthesis and review. *Earth-Sci. Rev.,* **75**, 85–104

Andrews, J.E. and Brasier, A.T. 2005. Seasonal records of climatic change in annually laminated tufas: short review and future prospects. *J. of Quat. Sci.* **20**(5), 411–421

Andrews, J.E., Riding, R., Dennis, P.F. 1993. Stable isotopic compositions of Recent freshwater cyanobacterial carbonates from the British Isles: local and regional environmental controls. *Sedimentology*, **40**, 303–314

Andrews, J.E., Pedley, H.M., Dennis, P. 2000. Palaeoenvironmental records in Holocene Spanish tufas: stable isotope approach in search of reliable climatic archives. *Sedimentology*, **47**, 961–978

Anwar, E.A.A. 2004. Petrography, geochemistry and genesis of tufa deposits of Bir Dungul area, South Western Desert, Egypt. *Sedim. of Egypt.*, **12**, 131–147

Arenas, C., Gutierrez, F., Osácar, C., Sancho, C. 2000. Sedimentology and geochemistry of fluvio-lacustrine tufa deposits controlled by evaporite solution subsidence in the central Ebro Depression, NE Spain. *Sedimentology*, **47**, 883–909

Arenas-Abad, C., Vázquez-Urbez, M., Pardo-Tirapu, G., Sancho-Marcén, C. 2010. Fluvial and associated carbonate deposits. In: Alonso-Zarza, A., Tanner, L.H. (Eds.) Carbonates in continental settings: processes, facies and application. *Dev. Sedimentol.*, **61**, 133–175

Armitage, S.J., Drake, N.A., Stokes, S., El-Hawat, A., Salem, M.J., White, K., Turner, P., McLaren, S.J. 2007. Multiple phases of North African humidity recorded inn lacustrine sediments from the Fazzan Basin, Libyan Sahara. *Quat. Geochron.* **2**, 181–186

Bakri, A.E., Tantawi, A., Blavoux, B., Dray, M. 1992. Sources of water recharge identified by isotopes in El Minya Governate (Nile Valley, Middle Egypt). In "Isotope Techniques in Water Resources Development 1991: Proceedings of an International Symposium on Isotope Techniques in Water Resources Development," 643−644 International Atomic Agency, Vienna.

Bar-Matthews, M., Ayalon, A., Gilmour, M., Matthews, A., Hawkesworth, C.J. 2003. Sea-land oxygen isotopic relationships from planktonic foraminifera and speleothemes on the Eastern Mediterranean region and their implications for paleorainfall during interglacial intervals. *Geochem. Cosmochim. Acta,* **67**, 3181–3199

Berger, A., Loutre, M.F., Crucifix, M. 2003. The Earth's climate in the next hundred thousand years. *Surveys in Geophysics*, **24**, 117–138

Bosmans, J.H.C., Drijfhout, S.S., Tuenter, E., Hilgen, F.J., Lourens, L.J. 2015. Precession and obliquity forcing of the freshwater budget over the Mediterranean. *Quat. Sci. Rev.,* **123**, 16–30

Bottinga, Y. 1968. Calculation of fractionation factors for carbon and oxygen isotopic exchange in the system calcite–carbon dioxide–water. *Journal of Physical Chemistry*, **72**, 800–808

Bowen, G.J. 2008. The Online Isotopes in Precipitation Calculator. OIPC2.2 (7/2008) Available from: http://www.waterisotopes.org

Brand, W.A., Assonov, S.S., Coplen, T.B. 2010. Correction for the ^{17}O interference in $\delta(^{13}C)$ measurements when analyzing CO_2 with stable isotope mass spectrometry (IUPAC Technical Report). *Pure Appl. Chem.*, **82**, 1719–1733

Brook, G.A., Embabi, N.S., Ashour, M.M., Edwards, R.L., Cheng, H., Cowart, J.B., Dabous, A.A., 2002. Djara cave in the Western desert of Egypt: morphology and evidence of Quaternary climatic change. *Cave Karst Sci*., **29**, 57–66

Brookes, I.A. 2010. Spatially variable sedimentary responses to orbitally driven plu-vial climate during marine oxygen isotope stage 5.1, Dakhla Oasis region, Egypt. *Quat. Res.*, **74**, 252–264

Burgener, L., Huntington, K.W., Hoke, G.D., Schauer, A., Ringham, M.C., Latorre, C., Díaz, F.P. 2016. Variations in soil carbonate formation and seasonal bias over >4 km of relief in the western Andes (30_S) revealed by clumped isotope thermometry. *Earth Planet. Sci. Lett.*, **441**, 188–199

Burns, S.J., Matter, A. 1995. Geochemistry of carbonate cements in surficial alluvial conglomerates and their paleoclimatic implications, Sultanate of Oman. *J. of Sed. Res.* **A65** (1), 170–177

Burns, S.J., Fleitmann, D., Mattter, A., Neff, U., Mangini, A. 2001. Speleothem evidence from Oman for continental pluvial events during interglacial periods. *Geology*, **29**, 623–626

Butzer, K.W. 1964. Pleistocene palaeoclimates of the Kurkur Oasis, Egypt. *Canadian Geographer*, VIII/3, 125–141

Butzer, K.W. 1965. Desert landforms at the Kurkur Oasis, Egypt. *Assoc. Geogr.*, **55**, 578–591

Cancellieri, E., Cremaschi, M., Zerboni, A., di Lernia, S. 2016. Climate, Environment, and Population Dynamics in Pleistocene Sahara. In: Sacha C. Jones and Brian A. Stewart (eds.), *Africa from MIS 6-2: Population Dynamics and Paleoenvironments, Vertebrate Paleobiology and Paleoanthropology*. Springer (2016), 123–145

Capezzuoli, E., Gandin, A., Sandrelli, F. 2010. Calcareous tufa as indicators of climatic variability: a case from the Southern Tuscany (Italy). In: Pedley, M. & Rogerson, M. (eds). "Tufas, Speleothems and Stromatolites: Unravelling the Physical and Microbial Controls". *Geological Society London*, Special Publications **336**, 263–281

Capezzuoli, E., Gandin, A., Pedley, M. 2014. Decoding tufa and travertine (fresh water carbonates) in the sedimentary record: the state of the art. *Sedimentology*, **61**, 1–21

Chafetz, H.S., Folk, R.L. 1984. Travertines – depositional morphology and the bacterially constructed constituents. *J. Sed. Petrol.*, **54**, 289–316

Cheng, H., Edwards, R.L., Shen, C.-C., Polyak, V.J., Asmerom, Y., Woodhead, J., Hellstrom, J., Wang, Y., Kong, X., Spötl, C., Wang, X., Calvin Alexander J.E. 2013. Improvements in ^{230}Th dating, ^{230}Th and ^{234}U half-life values, and U–Th isotopic measurements by multi-collector inductively coupled plasma mass spectrometry. Earth and Planetary Science Letters, 371–372, 82–91

Churcher, C.S., Kleindienst, M.R., Schwarcz, H.P. 1999. Faunal remains from a Mid-dle Pleistocene lacustrine marl in Dakhleh Oasis, Egypt: palaeoenvironmental reconstructions. *Palaeogeogr. Palaeoclimatol. Palaeoecol.*, **154**, 301–312

Cremaschi, M., Zerboni, A., Spötl, C., Felletti, F. 2010. The calcareous tufa in the Tadrart Acacus Mt. (SW Fezzan, Libya) An early Holocene paleoclimate archive in the central Sahara. *Palaeogeogr. Palaeoclimatol. Palaeoecol.*, **287**, 81–94

Crombie, M.K., Arvidson, R.E., Sturchio, N.C., El Alfy, Z., Abu Zeid, K. 1997. Age and isotopic constraints on Pleistocene pluvial episodes in the Western Desert, Egypt. *Palaeogeogr., Palaeoclim., Palaeoecol.* **130**, 337–355

Dabous, A.A., Osmond, J.K. 2001. Uranium isotopic study of artesian and pluvial contributions to the Nubian Aquifer, Western Desert. *Egypt. J. Hydrol.*, **243**, 242–253

Dal Sasso, G., Zerboni, A., Maritan, L., Angelini, I., Compostella, C., Usai, D., Artioli, G. 2018. Radiocarbon dating reveals the timing of formation and development of pedogenic calcium carbonate concretions in Central Sudan during the Holocene. *Geochim. Cosmochim. Acta*, **238**, 16–35

De Boever, E., Brasier, A.T., Foubert, A., Kele, S. 2017. What do we really know about early diagenesis of non-marine carbonates? *Sed. Geol.*, **361**, 25–51

Della Porta, G. 2015. Carbonate build-ups in lacustrine, hydrothermal and fluvial settings: comparing depositional geometry, fabric types and geochemical signature. In: Bosence, D.W.J., Gibbons, K.A., Le Heron, D.P., Morgan, W.A., Pritchard, T., Vining, B.A. (Eds.), Microbial Carbonates in Space and Time: Implications for Global Exploration and Production, vol. 418. Geological *Society, London, Special Publications* 17–68

Della Porta, G., Capezzuoli, E., De Bernardo, A. 2017a. Facies character and depositional architecture of hydrothermal travertine slope aprons (Pleistocene, Acquasanta Terme, Central Italy). *Marine and Petr. Geol.*, **87**, 171–187

Della Porta, G., Croci, A., Marini, M., Kele, S. 2017b. Depositional architecture, facies character and geochemical signature of the Tivoli travertines (Pleistocene, Acque Albule Basin, Central Italy). *Rivista Italiana di Paleontologia e Stratigrafia* **123**(3), 487–540

Dennis, K.J., Affek, H.P., Passey, B.H., Schrag, D.P., Eiler, J.M. 2011. Defining an absolute reference frame for "clumped" isotope studies of CO_2. *Geochim. Cosmochim. Acta*, **75**, 7117–7131

Di Nezio, P.N., Timmermann, A., Tierney, J.E., Jin., F.F., Otto-Bliesner, B., Rosenbloom, N., Mapes, B., Neale, R., Ivanovic, R.F., Montenegro, A. 2016. The climate response of the Indo-Pacific warm pool to glacial sea level. *Paleoceanography*, **31**, 866–894

Drake, N.A., El-Hawat, A.S., Turner, P., Armitage, S.J., Salem, M.J., White, K.H., McLaren, S. 2008. *Palaeogeogr. Palaeoclimatol. Palaeoecol.*, **263**, 131–145

Drake, N.A., Blench, R.M., Armitage, S.J., Bristow, C.S., White, K.H. 2011. Ancient watercourses and biogeography of the Sahara explain the peopling of the desert. *Proc. Nat. Acad. Sci. Am.* **108**, 458–462

Drake, N. and Breeze, P. 2016. Climate Change and Modern Human Occupation of the Shara from MIS 6-2. In: Sacha C. Jones and Brian A. Stewart (eds.), *Africa from MIS 6-2: Population Dynamics and Paleoenvironments, Vertebrate Paleobiology and Paleoanthropology*. Springer (2016), 103–122

Drake, N.A., Breeze, P., Parker, A. 2013. Palaeoclimate in the Saharan and Arabian Deserts during the Middle Palaeolithic and the potential for hominin dispersals. *Quat. Int.*, **300**, 48–61

Dramis, F., Fubelli, G. 2015. Tufa Dams in Tigray (Northern Ethiopia) as Late Pleistocene-Holocene Climate Proxies. In: P. Billi (ed.), Landscapes and Landforms of Ethiopia, World Geomorphological Landscapes, DOI 10.1007/978-94-017-8026-1_11, Springer, 2015

Dramis, F., Fubelli, G., Calderoni, G., Esu, D. 2014. Holocene aggradation/degradation phases of tufa dams in northern Ethiopia and central Italy: a palaeoclimatic comparison between East Africa and Mediterranean Europe. *Zeitschrift für Geomorph.* **58**(4), 419–434

El-Shenawy, M.I., Kim, S.-T., Schwarcz, H.P., Asmerom, Y., Polyak, V.J. 2018. Speleothem evidence for the early human dispersal out of sub-Saharan Africa. *Quat. Sci. Rev.*, **188**, 67–76

Erthal, M.M., Capezzuoli, E., Mancini, A., Claes, H., Soete, J., Swennen, R. 2017. Shrub morpho-types as indicator for the water flow energy - Tivoli travertine case (Central Italy). *Sedimentary Geology*, **347**, 79–99

Fleitmann, D., Burns, S.J., Neff, U., Mangini, A., Matter, A. 2003. Changing moisture sources over the last 330,000 years in Northern Oman from fluid-inclusion evidence in speleothems. *Quaternary Research*, **60**, 223–232

Fleitmann, D., Burns, S.J., Pekala, M., Mangini, A., Al-Subbary, A., Al-Aowah, M., Kramers, J., Matter, A. 2011. Holocene and Pleistocene pluvial periods in Yemen, southern Arabia. *Quat. Sci. Rev.*, **30**, 783–787

Ford, T.D., Pedley, H.M. 1996. A review of tufa and travertine deposits of the world. *Earth Sci. Rev.*, **41**, 117–175

Gaber, A., Khalaf, F., Bastawisy, M., El-Baz, F. 2018. Combining satellite image data and field observations to characterize fresh-water carbonates in Kurkur Oasis, Southern Egypt. *J. of African Earth Sci.*, **139**, 193–204

Gandin, A., Capezzuoli, E. 2008. Travertine versus calcareous tufa: distinctive petrologic features and stable isotopes signatures. *It. J. of Quat. Sci.*, **21**, 125–136

Gandin, A., Capezzuoli, E. 2014. Travertine: Distinctive depositional fabrics of carbonates from thermal spring systems. *Sedimentology*, **61**, 264–290

Garnett, E.R., Gilmour, M.A., Rowe, P.J., Andrews, J.E., Preece, R.C. 2004. $^{230}Th/^{234}U$ dating of Holocene tufas: possibilities and problems. *Quat. Sci. Rev.*, **23**, 947–958

Gaven, C. 1982. Radiochronologie isotopique ionium–uranium. In: Le Shati, Lac Pleistocene du Fezzan (Libye). Laboratoire de Geologie du Quaternarie. Editions du Centre National de la Recherche Scientifique, Paris, pp. 44–54 (Chap IV).

Gaven, C., Hillaire-Marcel, C., Petit-Maire, N. 1981. A Pleistocene lacustrine episode in southeastern Libya. *Nature*, **290**, 131–133

Geyh, M.A., Thiedig, F. 2008. The Middle Pleistocene Al Mahru'qah Formation in the Murzuq Basin, northern Sahara, Libya: evidence for orbitally-forced humid episodes during the last 500,000 years. *Palaeogeogr. Palaeoclimatol. Palaeoecol.*, **257**, 1–21

Gossel, W., Ebraheem, A.M., Wycisk, P. 2004. A very large scale GIS-based ground-water flow model for the Nubian sandstone aquifer in eastern Sahara (Egypt, northern Sudan and eastern Libya). *Hydrogeol. J.* **12**, 698–713

Gossel, W., Sefelnasr, A., Weise, S.M., Friese, K., Stefanova, A., Wycisk, P. 2010. Hydrochemical and isotope analysis of deep groundwater from the Nubian Aquifer system in the Egyptian Oases. XXXVIII IAH Congress, Groundwater Quality Sustainability, Krakow, 12–17 September, 2010, extended abstracts, 1555–1559

Grant, K.M., Rohling, E.J., Bronk Ramsey, C., Cheng, H., Edwards, R.L., Florindo, F., Heslop, D., Marra, F., Roberts, A.P., Tamisiea, M.E., Williams, F. 2014. Seal-level variability over five glacial cycles. *Nature Comm.*, **5:5076**, DOI: 10.1038/ncomms6076

Grant, K.M., Grimm, R., Mikolajewicz, U., Marino, G., Ziegler, M. and Rohling, E.J. 2016. The timing of Mediterranean sapropel deposition relative to insolation, sea-level and African monsoon changes. *Quat. Sci. Rev.*, **140**, 125–141

Grant, K.M., Rohling, E.J., Westerhold, T., Zabel, M., Heslop, D., Konijnendijk, T., Lourens, L. 2017. A 3 million year index for NorthAfrican humidity/aridity and the implication of potential pan-African Humid periods. *Quat. Sci. Rev.*, **171**, 100–118

Hamdan, M.A., Brook, G.A. 2015. Timing and characteristics of the Late Pleistocene and Holocene wetter periods in the Eastern Desert and Sinai of Egypt, based on ^{14}C dating and stable isotope analysis of spring tufa deposits. *Quat. Sci. Rev.*, **130**, 168–188

Hamdan, M.A., Lucarini, G. 2013. Holocene paleoenvironmental, paleoclimatic and geoarchaeological significance of the Sheikh El-Obeiyid area (Farafra Oasis, Egypt). *Quat. Int.*, **302**, 154–168

Hancock, P.L., Chalmers, R.M.L., Altunel, E., Çakir, Z. 1999. Travitonics: using travertines in active fault studies. *J. of Structural Geol.*, **21**, 903–916

Hassan, K.M. 2014. Note on the isotopic geochemistry of fossil-lacustrine tufas in carbonate plateau – A study from Dungul region (SW Egypt). *Chemie der Erde*, **74**, 285–291

Hassan, K.M. 2015. Stable isotopic signatures of the modern land snail *Eremina desertorum* from a low-latitude (hot) dry desert – A study from the Petrified Forest, New Cairo, Egypt. *Chemie der Erde*, **75**, 65–72

Haynes, C.V., Haas, H. 1980. Radiocarbon evidence for Holocene recharge of groundwater, Western Desert, Egypt. *Radiocarbon*, **22**, 705–717

He, B., Olack, G., Colman, A. 2012. Pressure baseline correction and high-precision CO_2 clumped isotope (Δ_{47}) measurements in bellows and micro-volume modes. *Rapid. Commun. Mass Spectrom.*, **26**, 2837–2853

Hiess, J., Condon, D.J., McLean, N., Noble, S.R. 2012. $^{238}U/^{235}U$ Systematics in Terrestrial Uranium-Bearing Minerals. *Science*, **335**, 1610 (2012)

Hoffmann, D.L., Rogerson, M., Spötl, C., Luetscher, M., Vance, D., Osborne, A.H., Fello, N.M., Moseley, G.E. 2016. Timing and causes of North African wet phases during the last glacial period and implications for modern human migration. *Sci. Rep.*, **6**, 36367, DOI: 10.1038/srep36367

Horton, T.W., Defliese, W.F., Tripati, A.K., Oze, C. 2016. Evaporation induced ^{18}O and ^{13}C enrichment in lake systems: A global perpective on hydrologic balance effects. *Quat. Sci. Rev*. **131**, 365–379

Issawi, B. 1968. The geology of Kurkur Dungul area. General Egyptian organization for geological research and mining. *Geol. Surv. Pap.*, **46**, 1–102

Issawi, B., Francis, M., Youssef, A., Osman, R. 2009. The Phanerozoic of Egypt: a Geodynamic Approach. *The Egyptian Geological Survey, Special Publication*, **81**, 589

Jaffey, H., Flynn, K.F., Glendenin, L.E., Bentley, W.C., Essling, A.M. 1971. Precision Measurement of Half-Lives and Specific Activities of ^{235}U and ^{238}U. *Phys. Rev. C*, **4**, 1889

Jimenez, G. 2014. Travertine from Egypt's Western Desert: a Terrestrial Record of North African Paleohydrology and Paleoclimate during the Late Pleistocene (Master's thesis) University of New Mexico, 95 p.

Jones, B., Renaut, R.W. 2010. Calcareous spring deposits in continental settings. In: *Developments in Sedimentology: Carbonates in Continental Settings: Facies, Environments and Processes* (Eds A.M. Alonso-Zarza and L.H. Tanner), 177–224 Elsevier, Amsterdam

Joseph, A., Frangi, J.P., Aranyossy, J.F. 1992. Isotope characteristics of meteoric water and groundwater in the Sahelo-Sudanese zone. *J. Geophys. Res.*, **97**, 7543–7551

Kano, A., Hagiwara, R., Kawai, T., Hori, M., Matsuoka, J. 2007. Climatic conditions and hydrological change recorded in a high-resolution stable-isotope profile of a recent laminated tufa on a subtropical island, southern Japan. *J. of Sed. Res.* **77**, 59–67

Kele, S., Demény, A., Siklósy, Z., Németh, T., Mária, T., Kovács, M.B. 2008. Chemical and stable isotope compositions of recent hot-water travertines and associated thermal

waters from Egerszalók, Hungary: depositional facies and non-equilibrium fractionations. *Sed. Geol.*, **211**, 53–72

Kele, S., Özkul, M., Gökgöz, A., Fórizs, I., Baykara, M.O., Alçiçek, M.C., Németh, T. 2011. Stable isotope geochemical and facies study of Pamukkale travertines: new evidences of low temperature non-equilibrium calcite–water fractionation. *Sed. Geol.*, **238**, 191–212

Kele, S., Breitenbach, S.F.M., Capezzuoli, E., Meckler, A.N., Ziegler, M., Millan, I.M., Kluge, T., Deák, J., Hanselmann, K., John, M.C., Yan, H., Liu, Z., Bernasconi, S.M. 2015. Temperature dependence of oxygen- and clumped isotope fractionation in carbonates: A study of travertines and tufas in the 6–95 ºC temperature range. *Geochim. Cosmochim. Acta*, **168**, 172–192

Kele, S., Sallam, E., Capezzuoli, E., Rogerson, M., Wanas, H., Shen, C., Lone, M., Yu, T., Schauer, A., Huntington, K., 2020. Clumped isotope geochemistry of calcareous tufa deposits from the Kurkur-Dungul region (Southern Egypt), Version Version 1.0. Interdisciplinary Earth Data Alliance (IEDA). https://doi.org/10.26022/IEDA/111782. Accessed 2020-12-17.

Khamies, A.A., El-Tarras, M.M. 2010. Surface and subsurface structures of Kalabsha area, southern Egypt, from remote sensing, aeromagnetic and gravity data. *Egyptian J. of Remote Sensing and Space Sci.*, **13**, 43–52

Kim, S.-T., O'Neil, J.R. 1997. Equilibrium and nonequilibrium oxygen isotope effects in synthetic carbonates. *Geochim. Cosmochim. Acta*, **61**, 3461–3475

Kindermann, K., Bubenzer, O., Nussbaum, S., Riemer, H., Darius, F., Pllath, N., Smet-tan, U. 2006. Palaeoenvironment and Holocene land use of Djara, western desert of Egypt. *Quat. Sci. Rev.*, **25**, 1619–1637

Kleindienst, M.R., Churcher, C.S., McDonald, M.M., Schwarcz, H.P. 1999. Geography, geology, geochronology and geoarchaeology of the Dakhleh Oasis region: An interim report. OXBOW MONOGRAPH, 1–54

Kleindienst, M.R., Schwarcz, H.P., Nicoll, K.A., Churcher, C.S., Frizano, J., Giegengack, R., Wiseman, M.F. 2008. Water in the Desert: First Report on Uranium-Series Dating of Caton-Thompson's and Gardner's 'Classic' Pleistocene Sequence at Refuf Pass, Kharga Oasis. In M. F. Wiseman, ed., The Oasis Papers 2. Proceedings of the Second International Conference of the Dakhleh Oasis Project. Oxford: Oxbow Books, 25–54

Kleindienst, M.R., Blackwell, B., Skinner, A.R., Churcher, C.S., Kieniewicz, J.M., Smith, J.R., Wise, N.L., Long, R.A., Deely, A.E., Blickstein, J. 2016. Assessing long-term habitability at an eastern Sahara oasis: ESR dating of molluscs and herbivore teeth at Dakhleh Oasis, Egypt. *Quat. Int.*, **408**, 106–120

Laskar, J., Robutel, P., Joutel, F., Gastineau, M., Correia, a. C.M., Levrard, B. 2004. A long-term numerical solution for the insolation quantities of the Earth. *Astron. Astrophys. Nor.*, **428**, 261–285

Linstadter, J., Kropelin, S. 2004. Wadi Bakht revisited: Holocene climate change and prehistoric occupation in the Gilf Kebir region of the eastern Sahara, SW Egypt. *Geoarchaeology*, **19**, 753–778

Lisiecki, L.E., Raymo, M.E. 2005. A Pliocene-Pleistocene stack of 57 globally distributed benthic $\delta^{18}O$ records. *Paleoceanography*, **20**, PA1003

McCool, J.-P. 2019. Carbonates as evidence for groundwater discharge to the Nile River during the Late Pleistocene and Holocene. *Geomorph.* **331**, 4–21

Mohammed, A. 2015. Deep Fluid Inputs into the Continental-Scale Nubian Sandstone Aquifer System Constrained by Hydrochemical, Stable Isotope, and Noble Gas Data. PhD thesis, Western Michigan University, Kalamazoo (MI).

Muller, A.B., Haynes, C.V. 1983. Isotope hydrology of the shallow groundwaters of the Western Desert. Proc. Int. Symp. on Isotope Hydrology. IAEA-SM-270/110P, 843–846

Nicoll, K., Sallam, E.S. 2017. Paleospring tufa deposition in the Kurkur Oasis region and implications for tributary integration with the River Nile in southern Egypt. *J. of African Earth Sci.*, **136**, 239–251

Nicoll, K., Giegengack, R., Kleindienst, M. 1999. Petrogenesis of Artifact-Bearing Fossil-Spring Tufa Deposits from Kharga Oasis, Egypt. *Geoarchaeology*, **14/8**, 849–863

Osmond, J.K., Dabous, A.A. 2004. Timing and intensity of groundwater movement during Egyptian Sahara pluvial periods by U-series analysis of secondary U in ores and carbonates. *Quat. Res.*, **61**, 85–94

Özkul, M., Kele, S., Gökgöz, A., Shen, C.-C., Jones, B., Baykara, M.O., Fórizs, I., Németh, T., Chang, Y.-W., Alçiçek, M.C. 2013. Comparison of the Quaternary travertine sites in the Denizli extensional basin based on their depositional and geochemical data. *Sed. Geol.*, **294**, 179–204

Pachur, H., Hoelzmann, P. 1991. Paleoclimatic implications of late Quaternary lacustrine sediments in western Nubia, Sudan. *Quat. Res.*, **36**, 257–276

Panichi, C., Tongiorgi, E. 1976. Carbon isotopic composition of CO_2 from springs, fumaroles, mofettes and travertines of central and southern Italy: a preliminary prospection method of geothermal area. Proc. 2nd UN Symposium on the Development and Use of Geothermal Energy. San Francisco, U.S.A., pp. 815–825 Pentecost, A., 2005. Travertine, Geologist Association. Springer-Verlag, Berlin, p. 445.

Patterson, L.J., Sturchio, N.C., Kennedy, B.M., van Soest, M.C., Sultan, M., Lu, Z.-T., Lehmann, B., Purtschert, R., Alfy, El, Z., Kaliouby, El, B., Dawood, Y., and Abdallah, A. 2005. Cosmogenic, radiogenic, and stable isotopic constraints on groundwater residence time in the Nubian Aquifer, Western Desert of Egypt: *Geochem., Geophys., Geosys.*, **6**(1), p. n/a–n/a, doi: 10.1029/2004GC000779.

Pazdur, A., Pazdur, M.F., Starkel, L., Szulc, J. 1988. Stable isotopes of Holocene calcareous tufa in southern Poland as paleoclimatic indicators. *Quat. Res.* **30**, 177–189

Pedley, H.M. 1990. Classification and environmental models of cool freshwater tufas. *Sed. Geol.*, **68**, 143–154

Pedley, M. 2009. Tufas and travertines of the Mediterranean region: a testing ground for freshwater carbonate concepts and developments. *Sedimentology*, **56**, 221–246

Pentecost, A. 2005. Travertine. Springer-Verlag, Berlin/Heidelberg, 445 p.

Petersen, S.V., Defliese, W.F., Saenger, C., Daëron, M., John, C.M., Huntington, K.W., Kelson, J.R., Bernasconi, S.M., Colman, A.S., Kluge, T., Olack, G.A., Schauer, A.J., Bajnai D., Bonifacie, M., Breitenbach, S.F.M., Fiebig, J., Fernandez, A.B., Henkes, G.A., Hodell, D., Katz, A., Kele, S., Lohmann, K.C., Passey, B.H., Petrizzo, D.A., Rosenheim, B.E., Tripati, A.E., Venturelli, R., Young, E.D., Wacker, U. and Winkelstern, I.Z. 2019. Effects of Improved ^{17}O Correction on Inter-Laboratory Agreement in Clumped Isotope Calibrations, Estimates of Mineral-Specific Offsets, and Temperature Dependence of Acid Digestion Fractionation. *Geochemistry, Geophysics, Geosystems*, Doi: 10.1029/2018GC008127, 1–42 p.

Pla-Pueyo, S. Viseras, C., Henares, S., Yeste, L.M., Candy, I. 2017. Facies architecture, geochemistry and palaeoenvironmental reconstruction of a barrage tufa reservoir analog (Betic Cordillera, S. Spain). *Quat. Int.*, **437**, 15–36

Railsback, L.B., Gibbard, P.L., Head, M.J., Voarintsoa, Ny Riano G. 2015. An optimized scheme of lettered marine isotope substages for the last 1.0 million years, and the

climatostratigraphic nature of isotope stages and substages. *Quat. Sci. Rev.*, **111**, 94–106

Ricketts, J.W., Ma, L., Wagler, A.E., Garcia, V.H. 2019. Global travertine deposition modulated by oscillations in climate. *J. of Quat. Sci.*, 1–11

Rogerson, M., Dublyansky, Y., Hoffmann, D.L., Luetscher, M., Töchterle, P., Spötl, C. 2019. Enhanced Mediterranean water cycle ecxplains increased humidity during MIS 3 in North Africa. *Climate of the Past*, **15**, 1757–1769

Rossignol-Strick, M., Paterne, M. 1999. A synthetic pollen record of the eastern Mediterranean sapropels of the last 1 Ma: implications for the time-scale and formation of sapropels. *Marine Geology*, **153**, 221–237

Said, R. 1961. Tectonic framework of Egypt, and its influence on the distribution of foraminifera. *A.A.P.G. Bull.*, **45**, 198–218

Sallam, E.S., Ruban, D.A. 2019. Ancient tufa and semi-detached megaclasts from Egypt: evidence for sedimentary rock classification development. *Int. J. Earth Sci.*, **108**, 1615–1616

Sallam, E.S., Ponedelnik, A.A., Tiess, G., Yashalova, N.N., Ruban, D.A. 2018. The geological heritage of the Kurkur-Dungul area in southern Egypt. *J. of African Earth Sci.*, **137**, 103–115

Sanford, K.S. 1935. Sources of water in north-western Sudan. *Geographical Journal*, **85**, 412–431

Schauer, A.J., Kelson, J., Saenger, C., Huntington, K.W. 2016. Choice of ^{17}O correction affects clumped isotope (Δ_{47}) values of CO_2 measured with mass spectrometry. *Rapid Comm.* Mass Spec., **30**, 2607–2616

Shen, C.-C., Edwards, R.L., Cheng, H., Dorale, J.A., Thomas, R.B., Moran, S.B., Weinstein, S.E. and Edmonds, H.N. 2002. Uranium and thorium isotopic and concentration measurements by magnetic sector inductively coupled plasma mass spectrometry. *Chemical Geology*, **185**, 165–178

Shen, C.-C., Cheng, H., Edwards, R.L., Moran, S.B., Edmonds, H.N., Hoff, J.A. & Thomas, R.T. 2003. Measurement of attogram quantities of ^{231}Pa in dissolved and particulate fractions of seawater by isotope dilution thermal ionization mass spectroscopy. *Analytical Chemistry*, **75**, 1075–1079

Shen, C.-C., Li, K.-S. et al. 2008. Variation of initial $^{230}Th/^{232}Th$ and limits of high precision U–Th dating of shallow-water corals. *Geochimica et Cosmochimica Acta*, **72**, 4201–4223

Shen, C.-C., Wu, C.-C., Cheng, H., Edwards, R.L., Hsieh, Y-T., Gallet, I., Chang, C.-C., Li. T.-Y., Lam, D.D., Kano, A., Hori, M., Spötl, C. 2012. High-precision and high-resolution carbonate ^{230}Th dating by MC-ICP-MS with SEM protocols. *Geochimica et Cosmochimica Acta*, **99**, 71–86

Sherif, M.I., Sultan, M., Sturchio, N.C. 2019. Chlorine isotopes as tracers of solute origin and age of groundwaters from the Eastern Desert of Egypt. *Earth Planet. Sci. Lett.*, **510**, 37–44

Smith, J.R. 2001. Geoarchaeology, Stable-Isotope Geochemistry, and Geochronology of Fossil-Spring Tufas, Western desert, Egypt (PhD thesis). University of Pennsylvania, Philadelphia, 180 p.

Smith, J.R. 2012. Spatial and temporal variation in the nature of Pleistocene pluvial phase environments across North Africa. In: Hublin, J.-J., McPherron, S.P. (Eds.), Modern Origins: a North African Perspective. Springer, Netherlands, Dordrecht, 35–47

Smith, J.R., Giegengack, R., Schwarcz, H.P. 2004a Constraints on Pleistocene pluvial climates through stable-isotope analysis of fossil-spring tufas and associated

gastropods, Kharga Oasis, Egypt. *Palaeogeogr., Palaeoclim., Palaeoecol.,* **206**, 157–175

Smith, J.R., Giegengack, R., Schwarcz, H.P., McDonald, M.M.A., Kleindienst, M.R., Hawkins, A.L., Churcher, C.S. 2004b. A reconstruction of Quaternary pluvial environments and human occupations using stratigraphy and geochronology of fossil-spring tufas, Kharga Oasis, Egypt. *Geoarchaeol.,* **19**, 407–439

Smith, J.R., Hawkins, A.L., Asmerom, Y., Polyak, V., and Giegengack, R. 2007. New age constraints on the Middle Stone Age occupations of Kharga Oasis, Western Desert, Egypt. *J. of Human Evol.*, **52** (6), 690–701

Sonntag, C., Klitzsch, E., Löhnert, E.P., E1-Shazly, E.M., Münnich, K.O., Junghans, Ch., Thorweihe, U., Weistroffer, K., Swailem, F.M. 1978a. Paleoclimatic information from D and O-18 in C-14 dated north Saharan groundwaters: Groundwater formation in the past. Proc. Int. Symp. on Isotope Hydrology, IAEA, 569–580

Sonntag, C., Klitzsch, E., E1-Shazly, E.M., Kalinke, C., Münnich, K.O. 1978b. Palaoklimatische Information im Isotpengehalt Cl4-datierter Grundwasser: Kontinentaleffekt in D und O18. *Geol. Rundsch.*, **67**, 413–423

Sturchio, N.C., Du, X., Purtschert, R., Lehmann, B.E., Sultan, M., Patterson, L.J., Lu, Z.-T., Müller, P., Bigler, T., Bailey, K., O'Connor, T.P., Young, L., Lorenzo, R., Becker, R., El Alfy, Z., El Kaliouby, B., Dawood, Y., Abdallah, A.M.A. 2004. One million year old groundwater in the Sahara revealed by krypton-81 and chlorine-36. *Geophys. Res. Lett.*, **31**, L05503, 4 p.

Sultan, M., Sturchio, N., Hassan, F.A., Hamdan, M.A.R., Mahmood, A.M., Alfy, Z.E., Stein, T. 1997. Precipitation Source Inferred from Stable Isotopic Composition of Pleistocene Groundwater and Carbonate Deposits in the Western Desert of Egypt. *Quat. Res.*, **48**, 29–37

Swanberg, C.A., Morgan, P., Boulos, F.K. 1983. Geothermal potential of Egypt. *Tectonophysics*, **96**, 77–94

Szabo, B.J., McHugh, W.P., Schaber, G.G., and Haynes, C.V. 1989. Uranium-series dated authigenic carbonates and Acheulian sites in southern Egyp. *Science*, **243**, 1053–1056

Szabo, B.J., Haynes, C.V., Maxwell, T.A. 1995. Ages of Quaternary pluvial episodesdetermined by uranium-series and radiocarbon dating of lacustrine deposits of Eastern Sahara. *Palaeogeogr. Palaeoclimatol. Palaeoecol.,* **113**, 22–242

Talbot, M.R. 1990. A review of the palaeohydrological interpretation of carbon and oxygen isotopic ratios in primary lacustrine carbonates. *Chem. Geol.* **80**, 261–279

Talma, A.S., Netterberg, F. 1983. Stable isotope abundancies in calcretes. In: R.C.L. Wilson (ed.), Residual Deposits, Geol. Soc. London Spec. Pub., 13. London (Geological Society), 221–233

Teboul, P.-A., Durlet, C., Gaucher, E.C., Virgone, A., Girard, J.-P., Curie, J., Lopez, B., Camoin, G.F. 2016. Origins of elements building travertine and tufa: New perspectives provided by isotopic and geochemical tracers. *Sed. Geol.,* **334**, 97–114

Thiedig, F.M., Oezen, D., El-Chair, M., Geyh, M.M. 2000. The absolute age of the Quaternary lacustrine limestone of the Al Mahruqah formation—Murzuk Basin, Libya. In: Sola, M.A., Worsley, D. (Eds.), Geological Exploration in the Murzuk Basin. Elsevier, Amsterdam, pp. 89–116

Thorweihe, U. 1982. Hydrogeologie des Dakhla Bekens (Agypten). *Berliner Geowiss. Abh. A*, **38**, 1–53

Thorweihe, U. 1990. Nubian Aquifer System. In Said, R. (Ed.), The Geology of Egypt. A.A. Balkema, Rotterdam, 601–614

Toker, E. 2017. Quaternary fluvial tufas of Sarıkavak area, southwestern Turkey: Facies and depositional systems. *Quat. Int.,* **437**, 37–50

Török, Á., Mindszenty, A., Claes, H., Kele, S., Fodor, L., Swennen, R. 2017. Geobody architecture of continental carbonates: "Gazda" travertine quarry (Süttő, Gerecse Hills, Hungary). *Quat. Int.*, **437**, 164–185

Vaks, A., Bar-Matthews, M., Ayalon, A., Matthews, A., Frumkin, A., Dayan, U., Halicz, L., Almogi-Labin, A., Schilman, B. 2006. Paleoclimate and location of the border between Mediterranean climate region and the Saharo–Arabian Desert as revealed by speleothems from the northern Negev Desert, Israel. *Earth Planet. Sci. Lett.*, **249**, 384–399

Vaks, A., Bar-Matthews, M., Matthews, A., Ayalon, A., Frumkin, A. 2010. Middle-Late Quaternary paleoclimate of northern margins of the Saharan-Arabian Desert: reconstruction from speleothems of Negev Desert, Israel. *Quat. Sci. Rev.*, **29**, 2647–2662

Van Houten, F.B., Bhattacharyya, D.P., Mansour, S.E.I. 1984. Cretaceous Nubia Formation and correlative deposits, eastern Egypt: Major regressive-transgressive complex. *Geol. Soc. of America Bull.*, **95**, 397–405

Voss, C.I., Soliman, S.M. 2014. The transboundary non-renewable Nubian aquifer system of Chad, Egypt, Libya and Sudan: classical groundwater questions and parsimonious hydrogeologic analysis and modeling. *Hydrogeol. J.*, **22**, 441–468

Wanas, H.A. 2012. Pseudospherulitic fibrous calcite from the Quaternary shallow lacustrine carbonates of the Farafra Oasis, Western desert, Egypt: A primary precipitate with possible bacterial influence. *J. of African Earth Sci.*, **65**, 105–114

Wanas, H.A., Armenteros, I. 2019. Microbially-induced fluvial tufa in Gunna hills, Farafra Oasis, Egypt: Facies analysis and stable isotopes. *J. of African Earth Sci.*, **158**, 103515.

Williams, M.A.J., Williams, F.M., Duller, G.A.T., Munro, R.N., El Tom, O.A.M., Barrows, T.T., Macklin, M., Woodward, J., Talbot, M.R., Haberlah, D., Fluid, J. 2010. Late Quaternary floods and droughts in the Nile valley, Sudan: newevidence fromoptically stimulated luminescence and AMS radiocarbon dating. *Quat. Sci. Rev.* **29**, 1116–1137

Figure and table captions

Fig. 1 Geological map showing the rock units exposed at the Kurkur–Dungul area (after Issawi 1968). The inset map shows the study area within Egypt.

Fig. 2 Geological cross sections at Kurkur Oasis, at the Dungul Oasis area and at the Gebel El–Digm area, showing the altitude of the studied sites of each localities, U/Th age data (in red) and $T\Delta_{47}$ data (in blue).

Fig. 3 Stable carbon and oxygen isotope composition of all tufa and calcite samples. Average $\delta^{13}C$ and $\delta^{18}O$ values of the studied sites at Kurkur Oasis, Dineigil Oasis, Gebel El-Digm and Dungul Oasis are also indicated. The inset diagram shows the correlation between the $\delta^{13}C$ and $\delta^{18}O$ values at Kurkur Oasis (sites 1–7).

Fig. 4 a) Comparison of U/Th age data of the studied tufa samples with published age data: scarp foot depression sediments, Western Desert (Abotalib *et al.* 2019); playa sediments, Eastern Sahara, SW Egypt (Linstadter and Kropelin 2004); tufa, Kharga Oasis (Smith *et al*. 2004b); tufa, Kharga Oasis (Smith *et al.* 2007); playa sediments, Farafra Oasis (Hamdan and Lucarini 2013); tufa, spring and playa sediments, Dakhla Oasis (Brookes 2010); wadi and scarp tufa, Western Desert (Smith 2001); lacustrine sediments, Western Nubia, Sudan (Pachur and Hoelzmann 1991); tufa, travertine, calcite, Western Desert (Sultan *et al.* 1997); tufa, travertine, Kurkur Oasis (Crombie *et al*. 1997); tufa,

Dakhla Oasis (Kleindienst *et al.* 1999); tufa, Khaga Oasis: Refuff Pass (Kleindienst *et al.* 2008); tufa, Eastern Desert (Hamdan and Brook 2015); travertine, Dakhla Oasis (Kleindienst *et al.* 2008, Jimenez 2014). b) Eustatic sea level curve (Grant *et al.* 2014). c) Marine Isotope Stages (Lisiecki and Raymo 2005; Railsback *et al.* 2015). d) ODP967 wet-dry index (Grant *et al.* 2017), Probability Saharan Humidity (Drake *et al.* 2013), clusters of North Saharan lacustrine deposits (Geyh and Thiedig 2008), East Saharan lacustrine deposits (Szabo *et al.* 1995). e) Data of Susah cave, Libya (Hoffmann *et al.* 2016), Wadi Sannur cave, Egypt (El-Shenawy *et al.* 2018), Negev Desert, Israel (Vaks *et al.* 2010), Hoti cave, Oman (Burns *et al.* 2001), Mukalla cave, Yemen (Fleitmann *et al.* 2011). f) Summer insolation at 30 °N (Laskar *et al.* 2004, El-Shenawy *et al.* 2018). Mediterranean Sapropels are indicated based on Rossignol-Strick and Paterne (1999) and Vaks *et al.* (2010).

Fig. 5 Stable oxygen isotope values of Egyptian tufa of this study (black column) and other freshwater carbonates (white columns) and speleothems (grey columns) from the studied region and neighbouring areas based on Fig. 4 of El-Shenawy *et al.* (2018) and using $\delta^{18}O$ data published by Gaven *et al.* (1981), Crombie *et al.* (1997), Burns *et al.* (2001), Brook *et al.* (2002), Bar-Matthews *et al.* (2003), Vaks *et al*. (2006), Affek *et al*. (2008), Vaks *et al.* (2010), Cremaschi *et al.* (2010), Fleitmann *et al.* (2011), Affek *et al.* (2014), Rogerson *et al.* (2019).

Table 1 Stable and clumped isotope results and calculated $\delta^{18}O_{water}$ values using the equations of Kim and O'Neil (1997) and Kele *et al.* (2015). The $\delta^{18}O_{water}$ values were calculated from the Δ_{47}-based temperature values and from the measured $\delta^{18}O_{calcite}$ values. The calculated values are only estimations, since the distance between the sampling points and the vent of the spring (where the deposition reflects close to equilibrium conditions according to Kele *et al.* 2015) is not known, thus, kinetic effects could have been played a role during carbonate deposition. $\delta^{13}C_{CO2}$ values were calculated using both the empirical equation of Panichi and Tongiorgi (1976) and the theoretical equation of Bottinga (1968).

Table 2 Uranium and Thorium isotopic compositions and ^{230}Th ages for the tufa samples.

Table 3 Delays to forcing, as defined by Berger *et al.* (2003). Negative delays imply either that tufa formation is leading precession or that delay is similar to the length of the precession cycle.

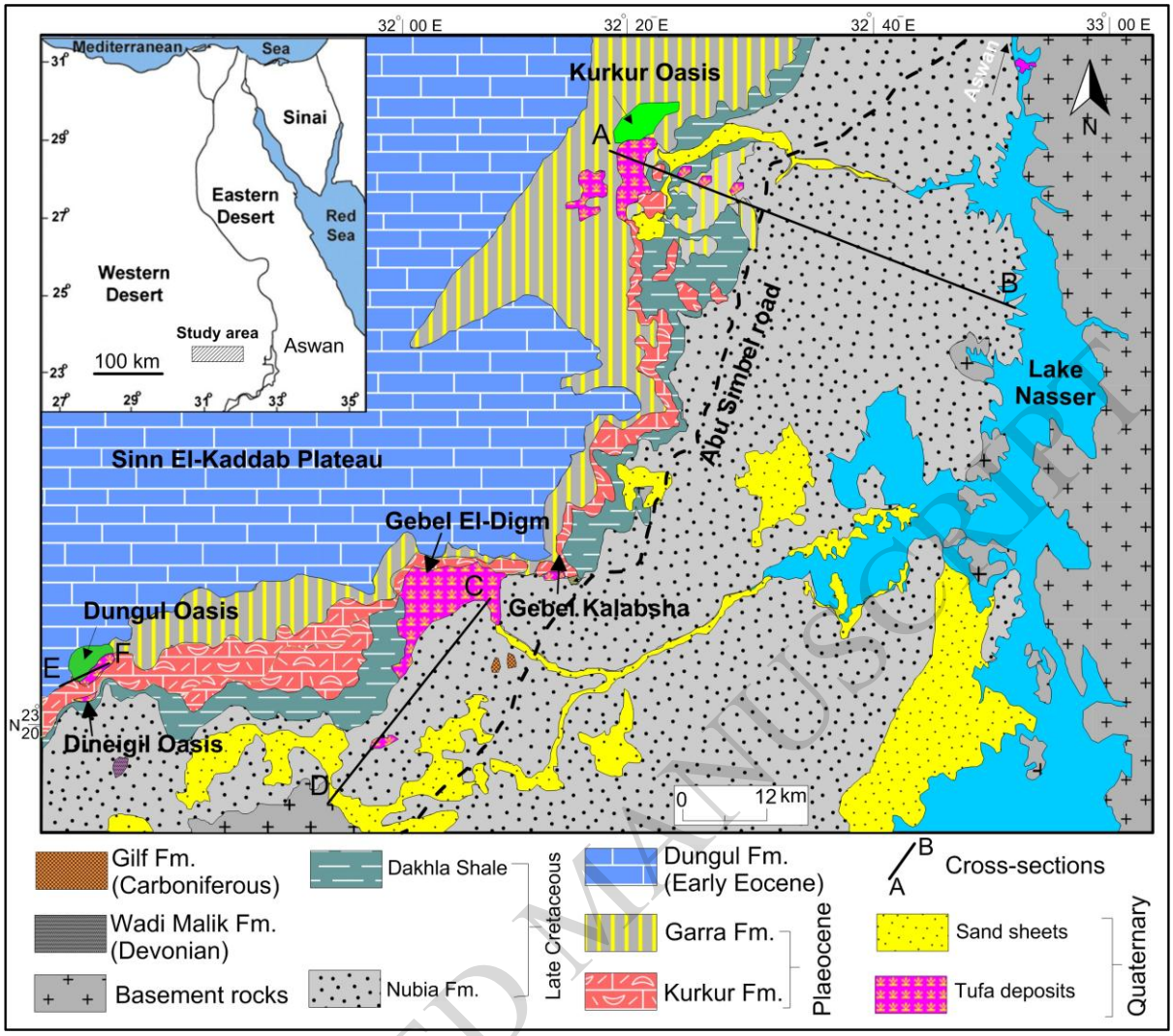

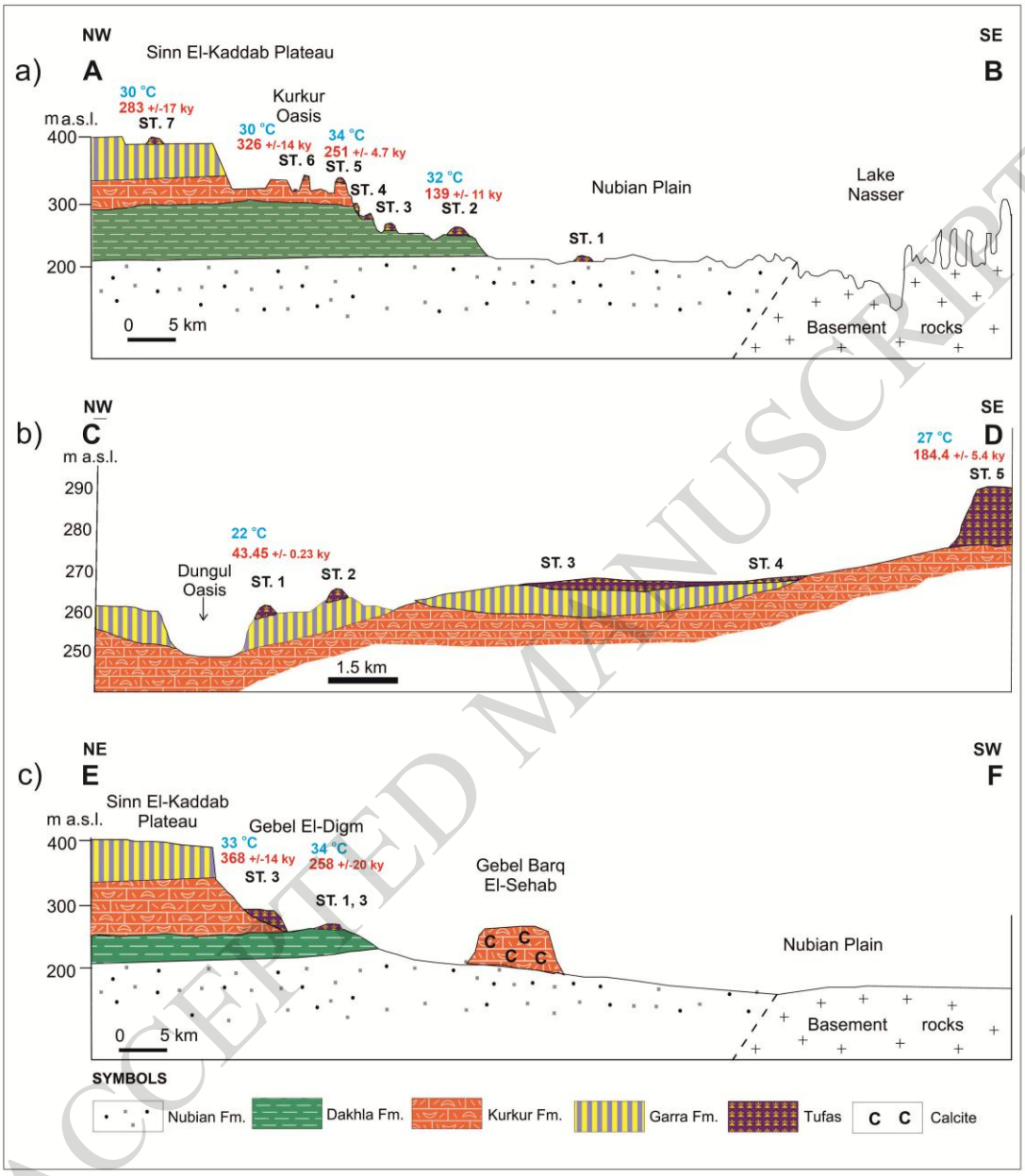

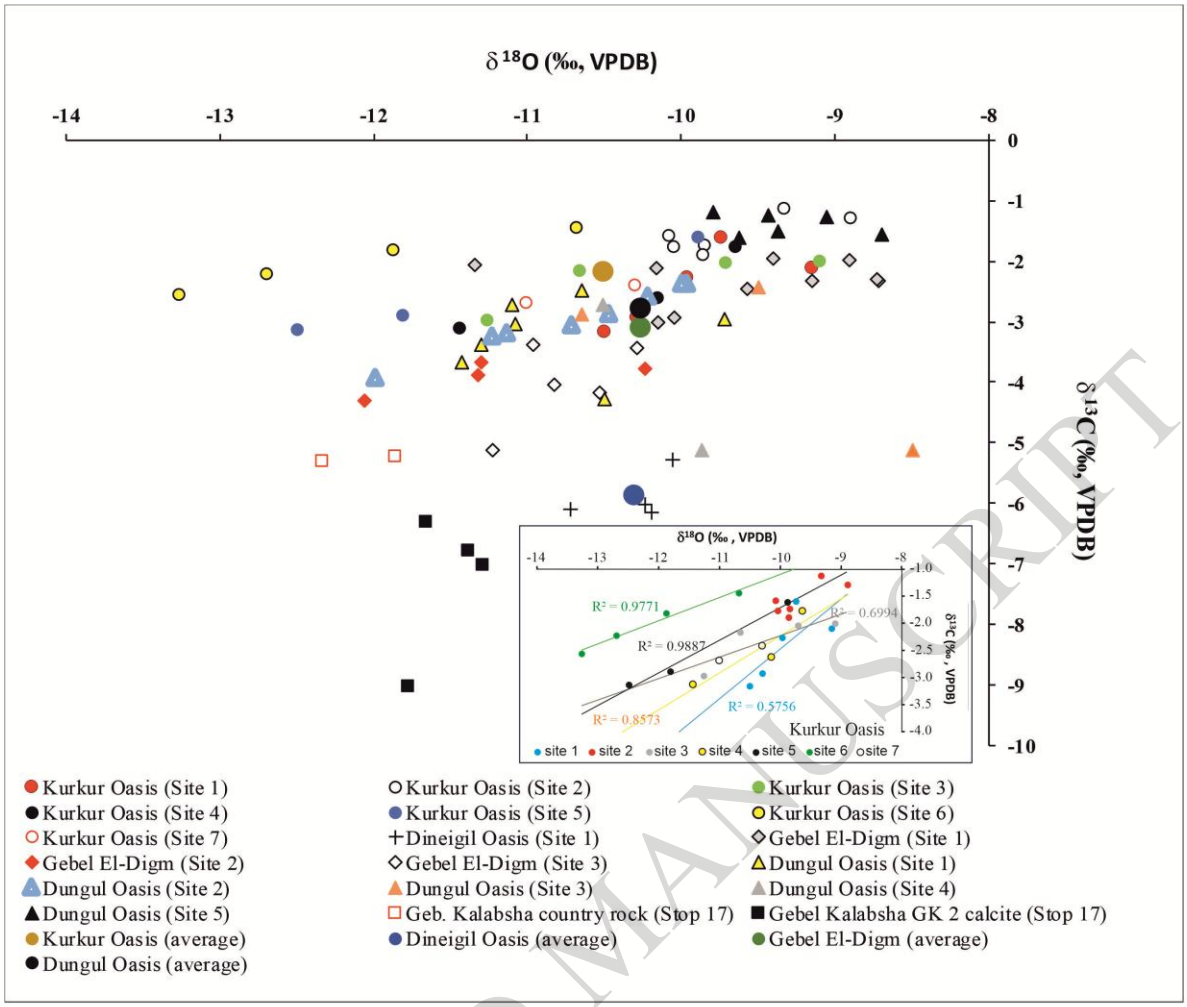

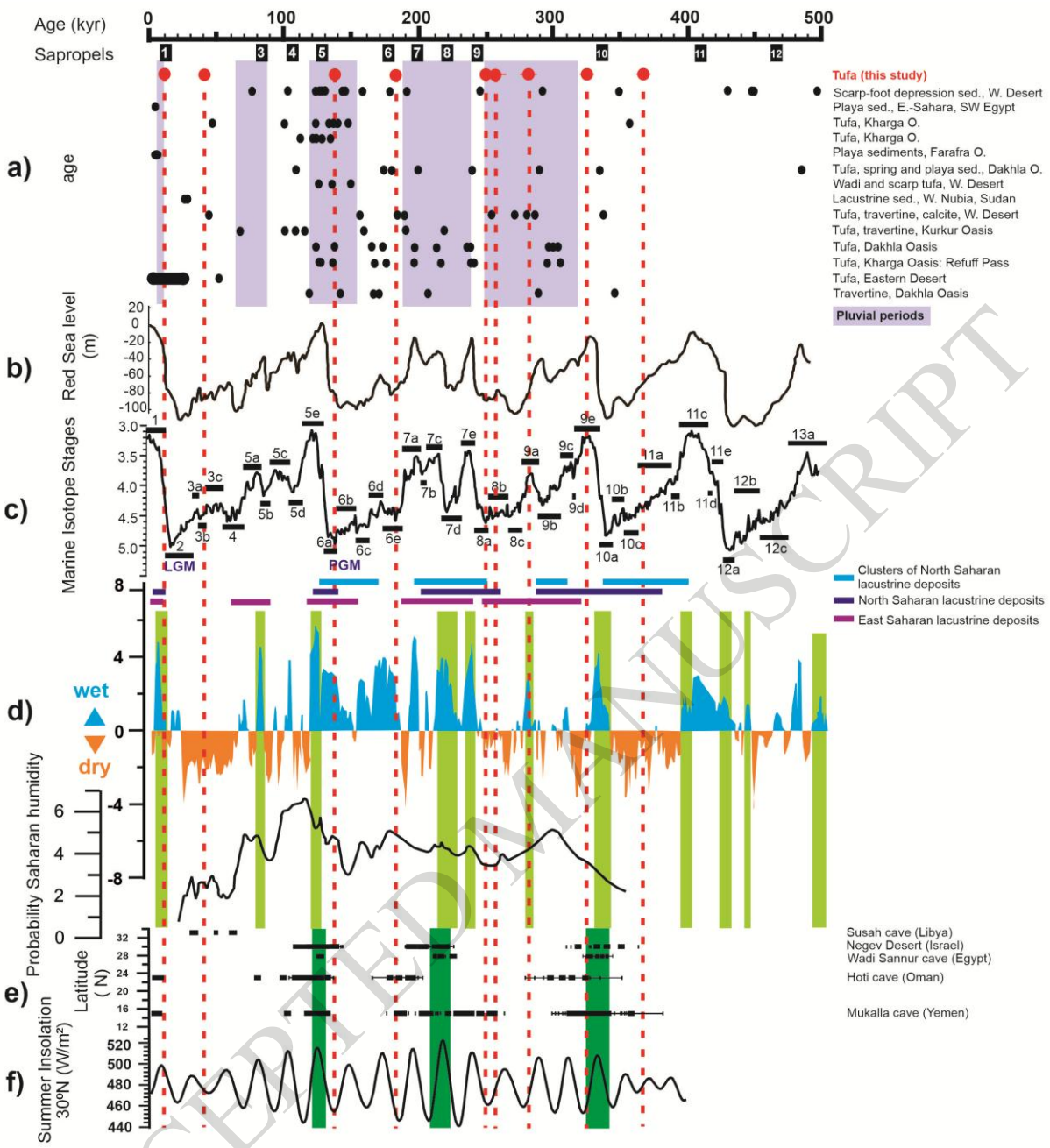

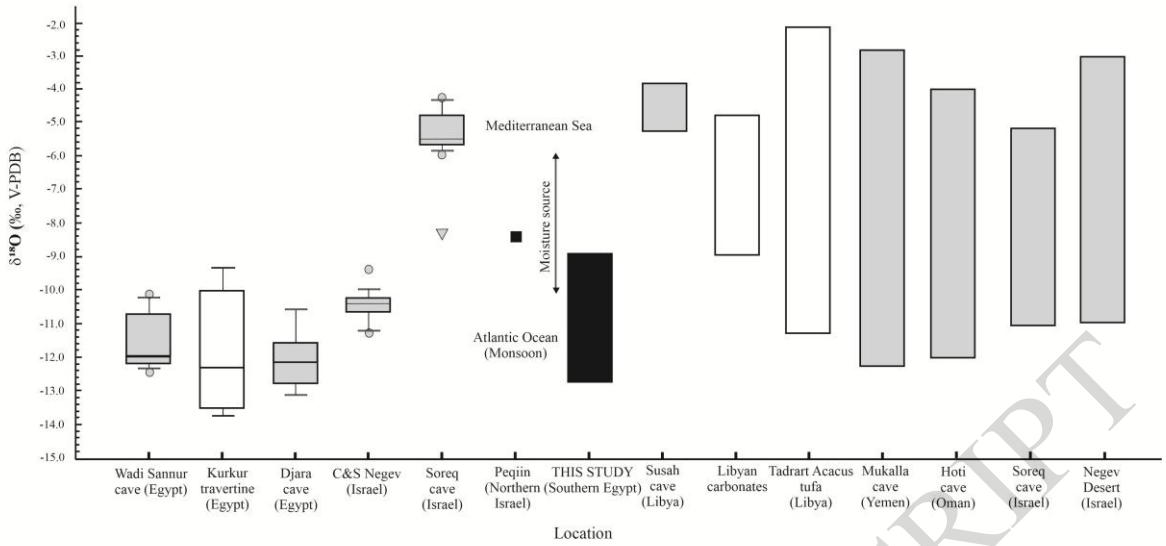

Table 1

Location	Sample ID	Repl.	$\delta^{13}C$ (V-PDB, ‰)	$\delta^{13}C$stdev	$\delta^{18}O$ (V-PDB, ‰)	$\delta^{18}O$stdev	Δ_{47} (‰)	Δ_{47} std error (‰)	T Δ_{47} (°C)	$\delta^{18}O_w$ [1]	$\delta^{18}O_w$ [2]	$\delta^{13}C_{CO2}$ [a]	$\delta^{13}C_{CO2}$ [b]
Kurkur	Kurkur 2-2	6	-1.60	0.018	-10.089	0.060	0.669	0.0184	32	-6.3	-8.7	-12.4	-11.0
Kurkur	Kurkur 5-2	6	-2.79	0.026	-11.994	0.051	0.664	0.0130	34	-7.8	-10.2	-13.9	-11.9
Kurkur	Kurkur 6-3	4	-2.17	0.008	-12.713	0.037	0.676	0.0099	30	-9.4	-11.8	-13.1	-11.9
Kurkur	Kurkur 7-1	4	-2.11	0.028	-9.640	0.062	0.676	0.0020	30	-6.3	-8.7	-13.0	-11.8
Dineigil	Dineigil 8-4	4	-5.93	0.025	-10.339	0.037	0.715	0.0116	16	-9.7	-11.9	-17.6	-17.5
Gebel El-Digm	Gebel El-D. 9-6	4	-1.85	0.016	-10.714	0.038	0.663	0.0017	34	-6.5	-8.9	-12.7	-11.0
Gebel El-Digm	Gebel El-D. 11-2	4	-4.32	0.015	-10.604	0.033	0.668	0.0059	33	-6.8	-9.1	-15.7	-13.7
Dungul	Dungul 12-1	3	-2.51	0.026	-9.595	0.094	0.699	0.0007	22	-7.9	-10.1	-13.5	-13.3
Dungul	Dungul 16-5	4	-1.47	0.027	-8.878	0.088	0.682	0.0048	27	-6.0	-8.3	-12.3	-11.5
Gebel Kalabsha	Gebel Kalab. 2-1	2	-6.18	0.012	-11.639	0.094	0.658	0.017	36	-7.1	-9.5	-17.9	-15.0

Δ_{47}-based temperature (T Δ_{47}) was calculated using the Petersen et al. (2019) equation.

$\delta^{18}O_{w\ and}$ $\delta^{18}O_w$ [2] was calculated using the equations of Kim and O'Neil (1997) and Kele et al. (2015), respectively.

$\delta^{13}C_{CO2}$ [a] have been calculated using the empirical equation of Panichi and Tongiorgi (1976).

$\delta^{13}C_{CO2}$ [b] have been calculated using the theoretical equation of Bottinga (1968)

Table 2

Sample ID	Weight g	^{238}U ppb[a]	^{232}Th ppt	$\delta^{234}U$ measured[a]	$[^{230}Th/^{238}U]$ activity[c]	$^{230}Th/^{232}Th$ atomic (x 10^{-6})	Age (kyr ago) uncorrected	Age (kyr ago) corrected[c,d]	Age (kyr BP) relative to 1950 AD	$\delta^{234}U_{initial}$ corrected[b]
Dineigil 8-4	0.1272	1135.1 ± 1.2	139525 ± 1312	431.1 ± 1.4	0.1729 ± 0.0033	23.20 #####	13.96 ± 0.28	11.7 ± 1.2	11.6 ± 1.2	445.6 ± 2.1
Kurkur 5-2	0.4405	883.82 ± 0.88	21934 ± 86	109.7 ± 1.2	1.0269 ± 0.0051	682.2 ± 4.2	251.6 ± 4.7	251.1 ± 4.7	251.0 ± 4.7	222.8 ± 4.0
Dungul 12-1	0.2683	3879.4 ± 5.9	17872 ± 58	241.1 ± 1.8	0.4139 ± 0.0016	1481.5 ± 7.2	43.62 ± 0.23	43.52 ± 0.23	43.45 ± 0.23	272.6 ± 2.0
Dungul 16-5	0.3727	186.24 ± 0.18	29370 ± 123	105.4 ± 1.5	0.928 ± 0.010	97.0 ± 1.1	188.0 ± 5.2	184.4 ± 5.4	184.4 ± 5.4	177.4 ± 3.8
Gebel El-Digm 9-6	0.3729	115.79 ± 0.10	67120 ± 442	61.5 ± 1.3	0.991 ± 0.017	28.19 #####	273 ± 21	258 ± 20	258 ± 20	127.3 ± 8.2
Gebel El-Digm 11-2	0.3210	102.31 ± 0.10	1317.6 ± 2.2	30.4 ± 2.2	1.0055 ± 0.0039	1287.3 ± 5.3	368 ± 14	368 ± 14	368 ± 14	85.9 ± 7.1
Kurkur 2-2	0.5044	221.03 ± 0.22	132486 ± 1311	61.9 ± 1.4	0.813 ± 0.019	22.37 #####	154.5 ± 7.9	139 ± 11	139 ± 11	91.6 ± 3.5
Kurkur 6-3	0.6033	320.86 ± 0.29	18315 ± 69	24.9 ± 1.1	0.9820 ± 0.0066	283.6 ± 2.2	328 ± 14	326 ± 14	326 ± 14	62.6 ± 3.8
Kurkur 7-1	0.4266	199.90 ± 0.23	28913 ± 178	65.4 ± 1.9	1.007 ± 0.013	114.8 ± 1.7	286 ± 18	283 ± 17	283 ± 17	145.3 ± 8.9
Dungul Calcite 22	0.7225	144.08 ± 0.43	7932 ± 38	25.9 ± 3.4	1.043 ± 0.014	312.4 ± 4.3	> 500	> 500	> 500	— —
Gebel Barq el Sehab-7	0.3135	80.10 ± 0.22	985.6 ± 4.5	-9.6 ± 4.4	0.985 ± 0.011	1320 ± 15	> 500	> 500	> 500	— —

Analytical errors are 2σ of the mean.

[a] $[^{238}U] = [^{235}U] \times 137.818$ (±0.65‰) (Hiess et al., 2012); $\delta^{234}U = ([^{234}U/^{238}U]_{activity} - 1) \times 1000$.

[b] $\delta^{234}U_{initial}$ corrected was calculated based on ^{230}Th age (T), i.e., $\delta^{234}U_{initial} = \delta^{234}U_{measured} X\ e^{\lambda 234 * T}$, and T is corrected age.

[c] $[^{230}Th/^{238}U]_{activity} = 1 - e^{-\lambda_{230}T} + (\delta^{234}U_{measured}/1000)[\lambda_{230}/(\lambda_{230} - \lambda_{234})](1 - e^{-(\lambda_{230} - \lambda_{234})T})$, where T is the age.

Decay constants are 9.1705×10^{-6} yr^{-1} for ^{230}Th, 2.8221×10^{-6} yr^{-1} for ^{234}U (Cheng et al., 2013), and 1.55125×10^{-10} yr^{-1} for ^{238}U (Jaffey et al., 1971).

[d] Age corrections, relative to chemistry date on November 21st, 2018, were calculated using an estimated atomic $^{230}Th/^{232}Th$ ratio of 4 (± 2) x 10^{-6}. Those are the values for a material at secular equilibrium, with the crustal $^{232}Th/^{238}U$ value of 3.8. The errors are arbitrarily assumed to be 50%.

Table 3

Sample ID	Age (kyr ago) corrected		Age of nearest NH insolation maximum	Delay to mean age (ka)
	Mean	Error		
Dineigil 8-4	11.7	± 1.2	10.3	-1.4
Kurkur 5-2	251.1	± 4.7	264.8	13.8
Dungul 12-1	43.52	± 0.23	57	13.4
Dungul 16-5	184.4	± 5.4	198.2	13.7
Gebel El-Digm 9-6	258	± 20	264.8	6.8
Gebel El-Digm 11-2	368	± 14	371.2	3.5
Kurkur 2-2	139	± 11	150	11.1
Kurkur 6-3	326	± 14	333.9	7.7
Kurkur 7-1	283	± 17	291.8	8.9
Smith et al., 2004	49.8	0.1	59.1	9.3
Smith et al., 2004	136	3	150	14
Smith et al., 2004	126	4	127.6	1.6
Smith et al., 2004	140	1.2	150	10
Smith et al., 2004	142	0.3	150	8
Smith et al., 2004	103	14	105.2	2.2
Smith et al., 2004	150	13	150	0
Smith et al., 2004	359	9	371.2	12.2
Smith et al., 2007	127.748	1.386	127.6	-0.2
Smith et al., 2007	129.808	5.058	127.6	-2.2
Smith et al., 2007	127.892	1.3	127.6	-0.3
Smith et al., 2007	114.395	4.193	127.6	13.2
Smith et al., 2007	124.567	3.383	127.6	3
Smith et al., 2007	127.069	3.826	127.6	0.5
Smith et al., 2007	125.665	2.5	127.6	1.9
Smith et al., 2007	123.84	3.645	127.6	3.7
Smith et al., 2007	137.617	2.629	150	12.4
Smith et al., 2007	136.358	3.365	150	13.6
Smith et al., 2007	136.039	2.2	150	14
Smith et al., 2007	130.532	2.832	150	19.5